



OPEN Sustainable slag-based geopolymers incorporating styrofoam and Moringa leaves ash for mechanical enhancement and crystal violet adsorption

Soher A. Hashish✉, Essam A. Kishar, Doaa A. Ahmed, Sheren M. Ragei & Aya Allah M. Ebrahim

Synthetic dye contamination poses a significant threat to water resources, necessitating the development of efficient removal technologies. This study introduces a novel organic-inorganic modified geopolymer for effective Crystal violet (CV) dye extraction from aqueous solutions. Additionally, it addresses waste management challenges by incorporating industrial (Slag, Styrofoam) and agricultural (Moringa leaves ash) waste into geopolymer cement. Slag-based geopolymer composites were synthesized with varying concentrations (1, 3, and 6 wt%) of Styrofoam (SSF1, SSF3, SSF6) and moringa leaves ash (SMA1, SMA3, SMA6). The mechanical properties of these composites were assessed over a curing period of up to 180 days in 100% humidity. While the control geopolymer sample (S) demonstrated superior compressive strength of 58.9 MPa after 180 days of curing, the modified geopolymer composites exhibited notable mechanical stability, with SSF1 and SMA1 achieving strengths of 52.8 MPa and 47.5 MPa, respectively. Furthermore, the adsorption performance of the modified geopolymer composites toward CV was evaluated as an additional environmental application. Notably, all modified geopolymers surpassed the control in CV removal, with SSF6 exhibiting an outstanding adsorption capacity of 434.78 mg/g. These findings demonstrate the potential of modified geopolymer composites as a promising, sustainable, and high-performance material for wastewater treatment applications.

Keywords Slag geopolymer, Styrofoam, Moringa leaves ash, Crystal violet, Batch adsorption

Abbreviations

CV	Crystal violet
MLA	Moringa leaves ash
SF	Styrofoam
LSS	Liquid sodium silicate
GGBFS	Ground granulated blast furnace slag
CAH	Calcium aluminate hydrate
CSH	Calcium silicate hydrate
CASH	Calcium alumino silicate hydrate
NASH	Sodium ammonium silicate hydrate
XRD	X-ray diffraction
SEM	Scanning electron microscopy
FTIR	Fourier-transform infrared spectroscopy
BET	Brunauer-Emmett-Teller
BJH	Barrett-Joyner-Halenda
pHpzc	The point of zero charge
PC	Portland cement

Chemistry Department, Faculty of Women for Arts, Science and Education, Ain Shams University, Cairo 11757, Egypt. ✉email: soherhashish@yahoo.com

The demand for more environmentally friendly building materials, geopolymers have gained attention as a strong substitute for conventional Portland cement. While geopolymers and PC may share comparable qualities, geopolymers are particularly promising since they are derived from materials that require less energy and emit less CO₂, like calcined clay, or industrial byproducts such as fly ash and slag with alkali activators¹. Slag, a highly reactive aluminosilicate substance, is created during the iron production from iron ore. It has been used expansively in the creation of geopolymers². Beyond construction, we're urgently tackling the massive problem of Styrofoam waste. Styrofoam is a synthetic polymer made from monomers of the aromatic hydrocarbon styrene³. Its production reaches several million tons per year⁴. Millions of tons of this synthetic material are produced yearly, taking over 500 years to decompose and releases large amounts of ozone into the atmosphere during manufacture⁵. Innovative recycling efforts are exploring its potential as a binder^{6,7}, an adsorbent⁸ or even as aggregate in lightweight concrete, all aiming to reduce its environmental footprint⁹.

Nature also offers solutions, notably through *Moringa oleifera*, a fast-growing, drought-resistant tree¹⁰. Its seed powder shows promise in creating sustainable concrete, and its leaves, particularly when turned into biochar, are proving effective at purifying wastewater^{11–13}, including the removal of harmful dyes from textile effluent¹⁴.

Over the past few decades, rapid industrialization has turned water pollution into a serious environmental issue concern. This brings us to a significant environmental challenge: water pollution from industrial dyes like Crystal Violet (CV). These dyes are not only persistent in water but also harmful to aquatic life by blocking sunlight and hindering photosynthesis. Furthermore, CV exposure poses serious risks to human health, such as respiratory issues and skin irritation, and potential carcinogenic effects. Addressing the pollution caused by CV requires effective remediation strategies. Recent studies have explored various methods, including biodegradation using specific bacterial strains capable of breaking down CV into less toxic compounds and the adsorption method using eco-friendly adsorbents^{15–18}.

While various methods exist for cleaning wastewater^{19,20}, adsorption is highly regarded for its effectiveness, affordability, and simplicity²¹. Lately, researchers have focused on developing adsorbents that are environmentally friendly, inexpensive, and highly effective²². One promising alternative for this purpose is a geopolymer²². Recent breakthroughs in developing microporous and mesoporous geopolymers have greatly improved their ability to act as adsorbents, offering an eco-friendly path toward cleaner water and a healthier planet^{23,24}. Both metakaolin geopolymer and moringa slag based geopolymers, demonstrate significant ability to adsorb dye from aqueous solutions due to their porous structure and surface chemistry^{25,26}. Modifications such as incorporating waste charcoal powder enhance adsorption capacity by increasing surface area and functional group density, achieving ultrahigh adsorption capacities exceeding 2800 mg/g in some composites²⁷. These properties make geopolymers promising, efficient adsorbents for CV removal in wastewater treatment, although further research is needed to improve reusability and practical application²⁸. However, no research has explored the combined effects of agricultural waste, specifically *Moringa* leaves, and organic industrial waste, such as Styrofoam, in slag-based geopolymer cement for environmental applications.

This research investigates a sustainable attempt to waste valorization by using industrial (Slag, Styrofoam) and agricultural (*Moringa* leaves ash) byproducts. The study utilizes *Moringa* leaf ash (MLA), chosen for its high silica and alumina content, which enhances structural integrity and reactivity, and Styrofoam (SF) as a pore-forming agent. This method addresses environmental concerns related to waste disposal and promotes sustainability in construction. The study highlights the effects of different amounts of SF and MLA on the mechanical performance of slag-based geopolymer composites. Furthermore, the study assesses the adsorption capacity of these composites in treating industrial effluent contaminated with crystal violet (CV) dye. The results demonstrate the potential of these novel organic-inorganic slag-based geopolymers for water treatment, highlighting their dual function in waste valorization and environmental remediation.

The findings indicate that Styrofoam and *Moringa* leaf ash can be used to produce sustainable geopolymer composites with improved mechanical and adsorptive properties. Future research should focus on their applications in construction and environmental remediation to further improve the long-term sustainability of these composites.

Materials and methodology

Materials

Ground granulated blast furnace slag (GGBFS) with particles size smaller than 100 µm was provided from Nile Overseas Company (Cairo, Egypt). Styrofoam was collected from packaging materials. The collected Styrofoam was cleaned and sorted to remove contaminants. The *Moringa Oleifera* leaves were gathered from a tree in the El Haden Area (El Behera, Egypt). Sodium hydroxide (NaOH) flakes and liquid sodium silicate (LSS) were supplied by EL Goumhouria Chemical Company (Cairo, Egypt), and the Silica Egypt Company (Alexandria, Egypt). The silica ratio of SiO₂/Na₂O equals 2.80 and the composition of liquid sodium silicate is 11.7 wt% Na₂O, 32.8 wt% SiO₂, and 55.5 wt% H₂O. Chemically pure Crystal violet (molar weight = 408.0 g mol⁻¹, λ-max = 590 nm, purity of 99.0%) was supplied from Prolabo company (France) (Fig. 1). The entire experiment proceeded with distilled water. The Blaine surface area of ground granulated blast furnace slag is 4700 × 50 cm² per gram.

Figure 2 displays the XRD and FTIR spectra of the raw materials. The XRD spectrum of GGBFS indicates broad peaks at 2θ = 25–35, which are owing to the glassy phase's high active silica content. Weak crystalline peaks at 2θ = 29.12 and 31.25 confirm the presence of akermanite and gehlinitite. The FTIR spectrum of GGBFS displays typical characteristics of slag, with bands at 908 cm⁻¹ related to Si–O–T (T = Si or Al) asymmetric stretching vibration and 450–470 cm⁻¹ indicating Si–O–Si bending vibration mode.

Moringa leaves ash (MLA) exhibit quartz and albite as the main phases in the XRD spectrum and shows characteristic bands in the FTIR spectrum at 3431 cm⁻¹ (linked to the presence of –OH group), 1098 cm⁻¹

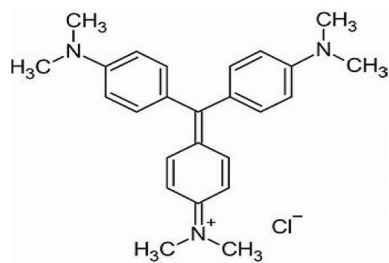


Fig. 1. Structure of crystal violet.

(linked to the vibrations of asymmetric Si-O-Si stretch), 874 cm^{-1} (vibrations of symmetrical stretching Si-O-Al), and 619 cm^{-1} (characteristic of crystalline cristobalite).

Styrofoam has an amorphous nature with a wide XRD signal around $2\theta = 20^\circ$ ²⁹. Its FTIR spectrum shows intense bands at 3026 cm^{-1} (indicating the presence of aromatic C-H), 2932 and 2852 cm^{-1} (representing aliphatic C-H), and 1600 and 1425 cm^{-1} (linked to C=C stretching). Additionally, there is a group of peaks below 1000 cm^{-1} (735 , 697 , and 538) due to the aromatic ring's C-H bending modes.

Geopolymer characterisation and methodology

Geopolymer composite preparation

Preparation of MLA The leaves of *Moringa oleifera* are collected from agricultural areas. To remove dirt and contaminants, the leaves were washed with clean water, dried for 24 h at 100°C , and then allowed to cool to room temperature. The dried leaves were crushed into small pieces using a mechanical crusher, followed by ultrafine grinding for a finer texture. The final powder was heated in an oven at 600°C for 2 h^{30,31} and sifted via a 100-mesh sieve to achieve a consistent particle size. The powdered moringa leaves were stored away from direct sunlight in a cool, dry place.

Preparation of alkaline activator The alkali, an activator solution, was made by mixing sodium hydroxide (10 M) and sodium silicate in a weight ratio of 2.5 and letting to cool for 24 h.

Synthesis of geopolymer Firstly, Styrofoam was dissolved in acetone to obtain a smooth paste⁷. To the dried mixtures, an alkaline activator solution was added and mixed for 15 min. Table 1 displays the constituents of the geopolymer composites. In order to enhance the mechanical properties in addition to adsorption characteristic, the maximum percentage chosen is 6% for both MLA and Styrofoam^{32,33}. After mixing, the sample pastes were poured into molds ($2.5\text{ cm} \times 2.5\text{ cm} \times 2.5\text{ cm}$), then cured for 24 h at 60°C . Following the curing period, the geopolymer cubes were removed from the molds and stored at 100% humidity. XRF was used to analyze the chemical oxide contents of ground granulated blast furnace slag and *Moringa Oleifera* leaves ash (MLA) in Table 2. The schematic diagram given in Fig. 3 summarizes a description of the preparation of geopolymer, characterization and adsorption test.

Characterization of geopolymer

To assess each paste's compressive strength, a D550-control type machine from Milan, Italy was used. An alcohol/acetone (1:1) solution was used to end the hydration process of the crushed cubic specimens and then dried for 24 h at 50°C . The total porosity of each hardened paste was assessed by Brunauer-Emmett-Teller (BET) surface area analyzer using the Quanta Chrome model of NOVA touch 2LX, Milano-Italy machine. High-resolution scanning electron microscopy (ESEM/Mapping; FEI, model Quanta FEG 250), infrared spectrophotometer (PerkinElmer 1430 infrared spectrophotometer, USA), and X-ray diffraction (Bruker D8 Discover diffractometer, Germany) were used to examine the phase composition, functional groups, microstructure, and morphological development of the hydration products. The textural characteristics were recognized using adsorption-desorption of the N_2 gas technique at 77°K using (MINI X, MICROTRAC). To calculate the average pore diameter (nm), specific surface area (m^2/g), and total pore volume (cm^3/g), Brunauer-Emmett-Teller (BET) and Barrett-Joyner-Halenda (BJH) models were employed.

Adsorption test

The removal efficiency and adsorption capacity of geopolymer composite mixes were studied using batch adsorption tests with varying crystal violet dye (CV) initial dye concentrations ($10\text{--}120\text{ mg L}^{-1}$), adsorbent dosages ($0.01\text{--}0.2\text{ g L}^{-1}$), contact time (30–360 min), and pH (2–8) at room temperature (25°C). The experiments were accomplished in batches using 50 mL dye solution in a shaker. A UV/visible spectrophotometer was used to quantify the concentration of the supernatant at $\lambda\text{-max} = 590\text{ nm}$. Equation (1) calculates the dye removal effectiveness (%), while Eqs. (2) and (3)³⁴ were used to quantify the adsorbed amount at equilibrium (q_e , mg g^{-1}), as well as the adsorbed quantity at a certain time t (q_t , mg g^{-1}).

$$R (\%) = \frac{(C_o - C_t)}{C_o} \times 100 \quad (1)$$

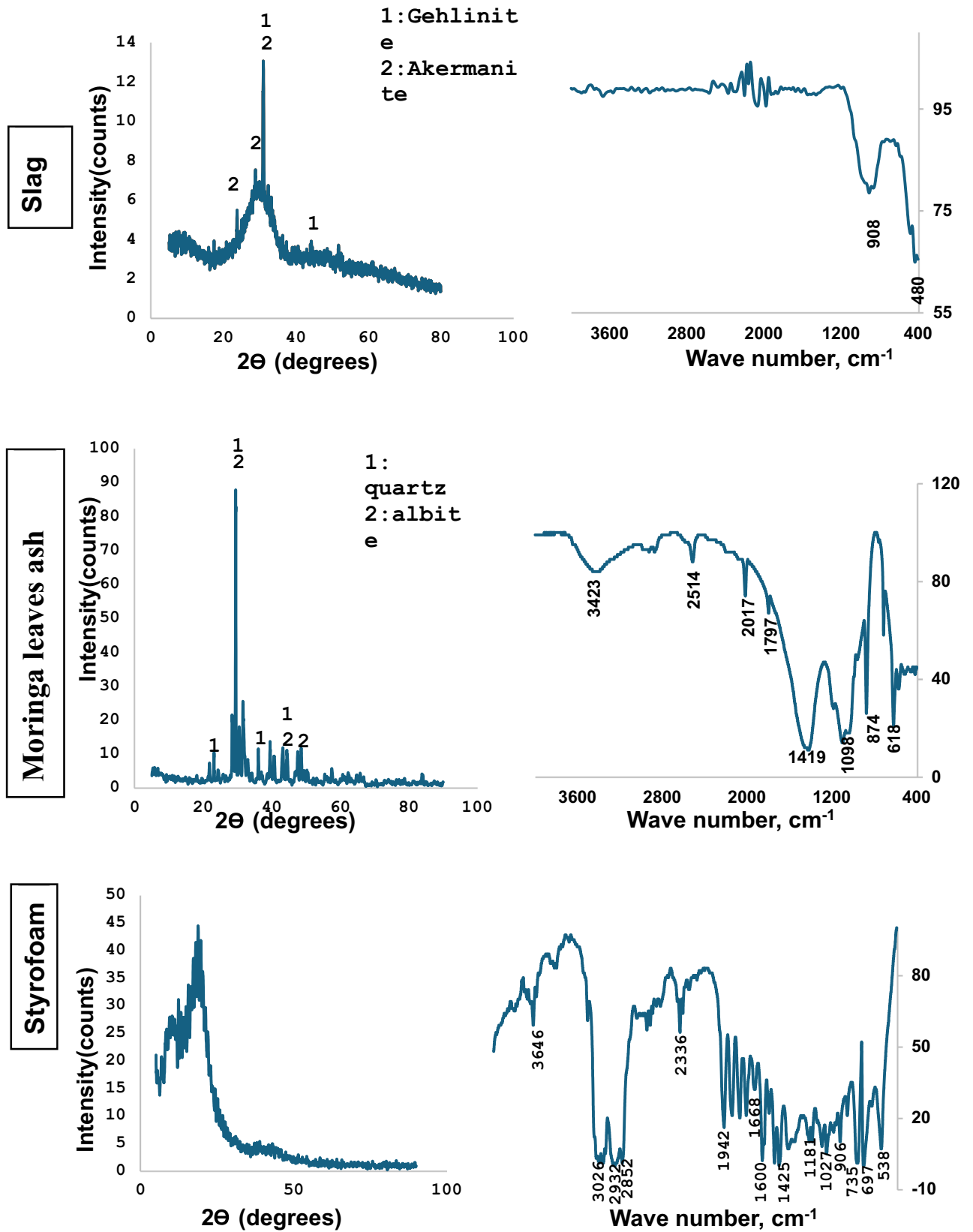


Fig. 2. The XRD and FTIR of raw materials.

Mix code	S	SMA1	SMA3	SMA6	SSF1	SSF3	SSF6
Wt. % of slag (GGBFS)	100%	99%	97%	94%	99%	97%	94%
Wt.% of Moringa leaves ash (MLA)	–	1%	3%	6%	–	–	–
Wt.% of styrofoam (SF)	–	–	–	–	1%	3%	6%

Table 1. The composition of the geopolymer paste mixes.

Chemical composition %											
	SiO ₂	Fe ₂ O ₃	CaO	Al ₂ O ₃	MgO	SO ₃	Na ₂ O	K ₂ O	L.O.I	Cl ⁻	H ₂ O
Slag	32.86	1.14	42.56	7.02	11.58	2.50	0.29	0.15	0.93	0	0
MLA	38.16	14.90	18.10	17.20	4.76	1.71	1.18	1.84	0.24	0.06	0

Table 2. Chemical oxide compositions (mass %).

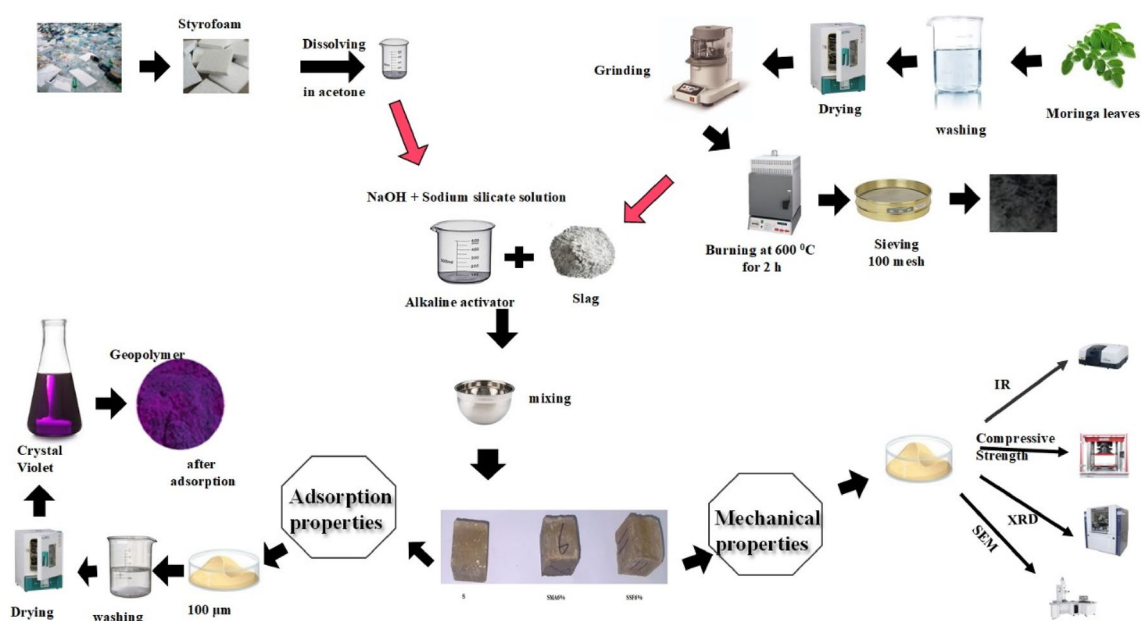


Fig. 3. Schematic diagram of the experimental process.

$$q_e = \frac{(C_o - C_e) v}{m} \quad (2)$$

$$q_t = \frac{(C_o - C_t) v}{m} \quad (3)$$

C_e (mg L⁻¹) is the concentration of adsorbate by an adsorbent at equilibrium, V is the volume of solution (L), m is the amount of adsorbent (g), and C_o (mg L⁻¹) is the initial concentration of dye and C_t (mg L⁻¹) concentration of the dye at time t .

Isotherm models

The equilibrium data obtained for CV on various prepared geopolymer mixes were modeled applying the Freundlich and Langmuir models. The linearized forms of the two isotherms are³⁴:

$$\frac{c_e}{q_e} = \frac{c_e}{q_m} + \frac{1}{k_1 q_m} \quad (4)$$

$$\ln q_e = \ln k_f + \frac{1}{n} \ln c_e \quad (5)$$

The equilibrium concentration is C_e (mg/L), while the amount of dye adsorbed at equilibrium is q_e (mg/g). The Langmuir constant is k_l (L/mg) while the monolayer adsorption capacity is q_m (mg/g). The maximum CV adsorbed into the geopolymer (q_m) and the Langmuir constant k_l was derived from the chart of C_e/q_e against C_e , as explained in Eq. (4). The Freundlich constants, k_f and n , represent the adsorption intensity and capacity, respectively. Similarly, the plot of $\ln(q_e)$ vs. $\ln(C_e)$, as shown in Eq. (5), can be utilized to obtain the Freundlich isotherm constants KF and n .

Kinetics models

Kinetic models are used in adsorption to explain how quickly adsorbents—such as particles, ions, or molecules—stick to an adsorbent's surface. The kinetics data produced on the adsorption investigation for the influence of time were examined in our investigation using pseudo-second-order model (Eq. 6), and the pseudo-first-order model (Eq. 7)³⁴.

$$\ln(q_e - q_t) = \ln q_e - \frac{k_1}{2.303}t \quad (6)$$

$$\frac{t}{q_t} = \frac{1}{k_2 q_e^2} + \frac{t}{q_e} \quad (7)$$

The amount of CV adsorbed at equilibrium is referred to as q_e (mg/g) and at times t by q_t (mg/g).

The pseudo-first-order adsorption rate constant is k_1 (min^{-1}) and the pseudo-second-order one is k_2 ($\text{g mg}^{-1} \text{min}^{-1}$).

Results and discussion

Mechanical characteristics

Compressive strength and total porosity%

The compressive strengths of the reference specimen and the geopolymeric composites containing MLA and Styrofoam up to 180 days are shown in Fig. 4. It is clear that the compressive strength rises with time due to the development in the geopolymerization process, resulting in the development of additional strength-giving phases in the existing open pores, including calcium aluminate hydrate (CAH), calcium silicate hydrate (C-S-H), calcium aluminosilicate hydrate (C-A-S-H), and sodium ammonium silicate hydrate (N-A-S-H)³⁵. By decreasing the porosity, the strength-giving phases create a compact matrix composite with superior mechanical properties as seen in Fig. 4. The mixes containing MLA gave lower compressive strength than the reference mix; this is properly due to the dilution of slag with less active pozzolanic material (MLA) and the lower dissolution of the silicate crystals (quartz and albite) encompassing the leaves' ash because of their higher stability³⁶. Furthermore, the MLA may cover the slag particles, preventing the slag from geopolymerizing³⁵. Mixes with Styrofoam show the lowest compressive strength and the highest porosity after 28 days. The findings are probably due to the deficiency of coherence between the Styrofoam fiber and the geopolymer matrix^{37,38}. So, incorporating MLA and SSF reduces the compressive strength and increases total porosity. Mix SMA6 and SSF6 will be further investigated to study their adsorption characteristics.

FTIR spectrum

The FT-IR spectra of the reference geopolymer paste (S) and the geopolymeric composite mixes (SMA6 and SSF6) at 7 and 180 days of hydration are shown in Fig. 5. All the samples were found to have seven transmittance bands at varying vibrational energies (cm^{-1}). Wide bands were found within the range of $3440\text{--}3460 \text{ cm}^{-1}$, that matches the symmetric stretching vibrations of the hydroxyl group³⁹. H-O-H bending vibrations or O-H bending vibrations are accountable for the bands observed around 1650 cm^{-1} ⁴⁰. The asymmetric and symmetric stretching vibrations of $-\text{CH}_2$ originating from the ash and Styrofoam of moringa leaves are linked to the two distinctive bands that emerged between 2920 and 2850 cm^{-1} ⁴¹. The bands at $1000\text{--}950 \text{ cm}^{-1}$ range were connected to Si-O-T asymmetric stretching vibration (where T is either Si or Al), which shifted to a lower wavenumber after 180 days. The bands around 875 cm^{-1} are frequently linked to the bending vibrations of the Si-O-Al bond in the geopolymer network. This is probably owing to the dissolution of active silica and the creation of more intricate and stable aluminosilicate networks, like those in C-S-H and C-A-S-H gels⁴². The peaks at $(659\text{--}674) \text{ cm}^{-1}$ relate to the symmetric Si-O-Si (Al) bridges' stretching vibrations in cyclo-silicates⁴³. However, the Si-O-Si bending vibration mode at approximately $(442\text{--}465) \text{ cm}^{-1}$ was related to unreacted quartz⁴⁴. During the carbonation process of $\text{Ca}(\text{OH})_2$, the C-O stretching vibration in CO_3^{2-} groups formed the bands at $1420\text{--}1450 \text{ cm}^{-1}$. The band at 875 cm^{-1} is slightly shifted because of the carbonation process that alters the chemical environment of the aluminosilicate network. From Fig. 5. It can be observed that mix SSF gives a more intense band at 1459 cm^{-1} after 180 days of hydration, which is probably because of its pores structure. While MLA shows a reduction in that peak, maybe due to the creation of more hydration products in the pores, which lowers the carbonation process.

X-ray diffraction

It is essential to understand the phases that result from geopolymerization, as they influence the adsorption and mechanical properties of geopolymeric composites. Figure 6 shows the phase composition of the synthetic geopolymer composites (S, SMA6, and SSF6). Different phases were identified within the reference and geopolymer composite's structure, aligned with the full dissolution of akermanite and gehlenite crystals presented in the pure GGBFS, such as sodium aluminosilicate hydrates (NASH) with known broadness between 22 and 35° because of the amorphous character of its chains, calcium aluminosilicate hydrates (CASH)

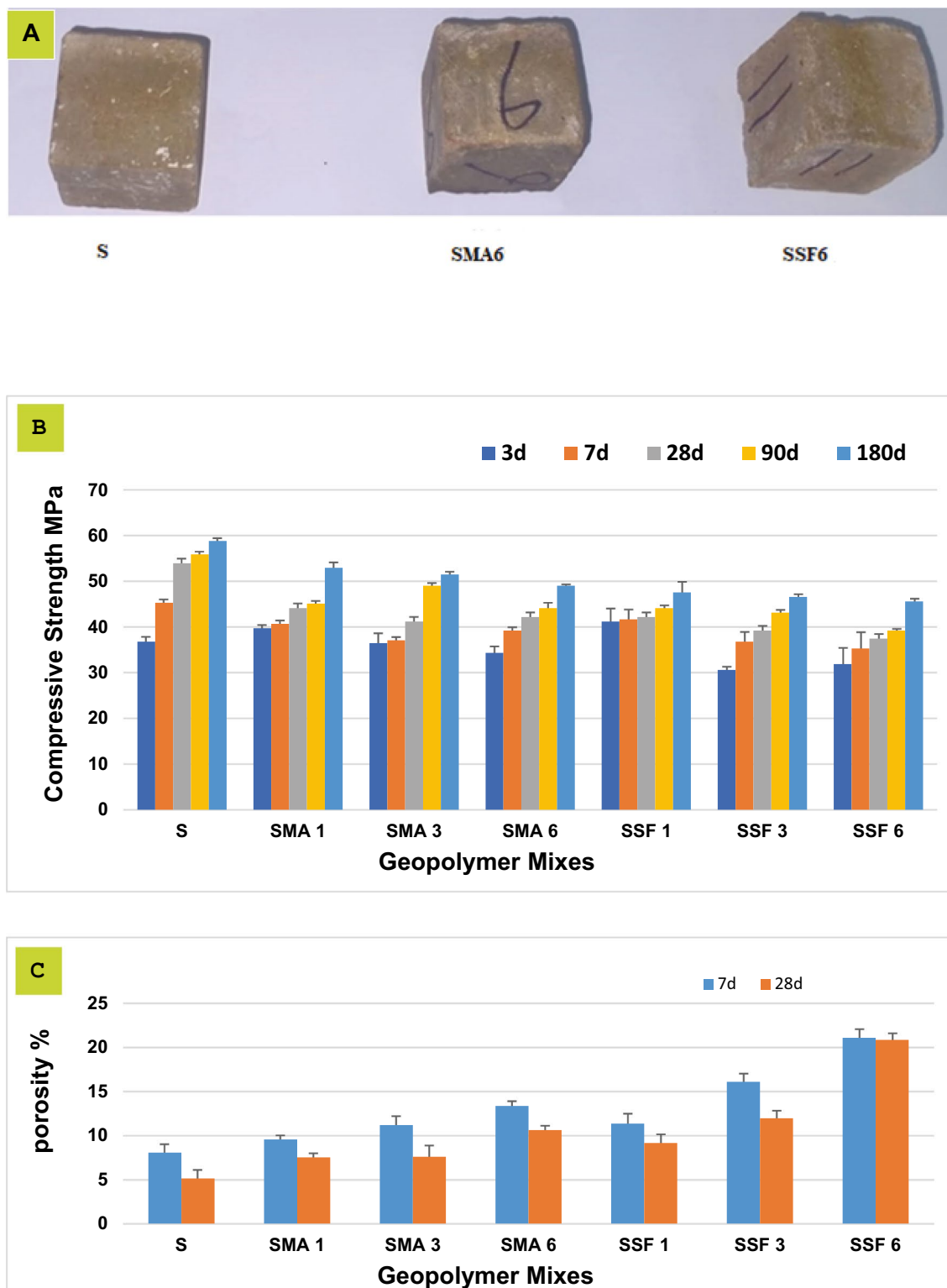


Fig. 4. (A) Geopolymeric cubes of three different compositions, (B) The values of compressive strength and (C) total Porosity % for the geopolymer at different ages.

at $2\theta=34, 44$ and 52° , calcium silicate hydrates (CSHs) at $2\theta=29^\circ$ and calcium alumina hydrates (CAH) at $2\theta=37$ and 51° ³⁴. Alkaline activation causes the precursor phases in the current geopolymer samples to dissolve significantly afterward polycondensation results in a more uniform aluminosilicate matrix, as indicated by the broadening or disappearance of the crystalline peaks (XRD of raw materials in Fig. 2). Early on, an amorphous hump of unreacted GGBFS was seen approximately at 30° , which corresponds to the C-S-H peak at 180 days. The

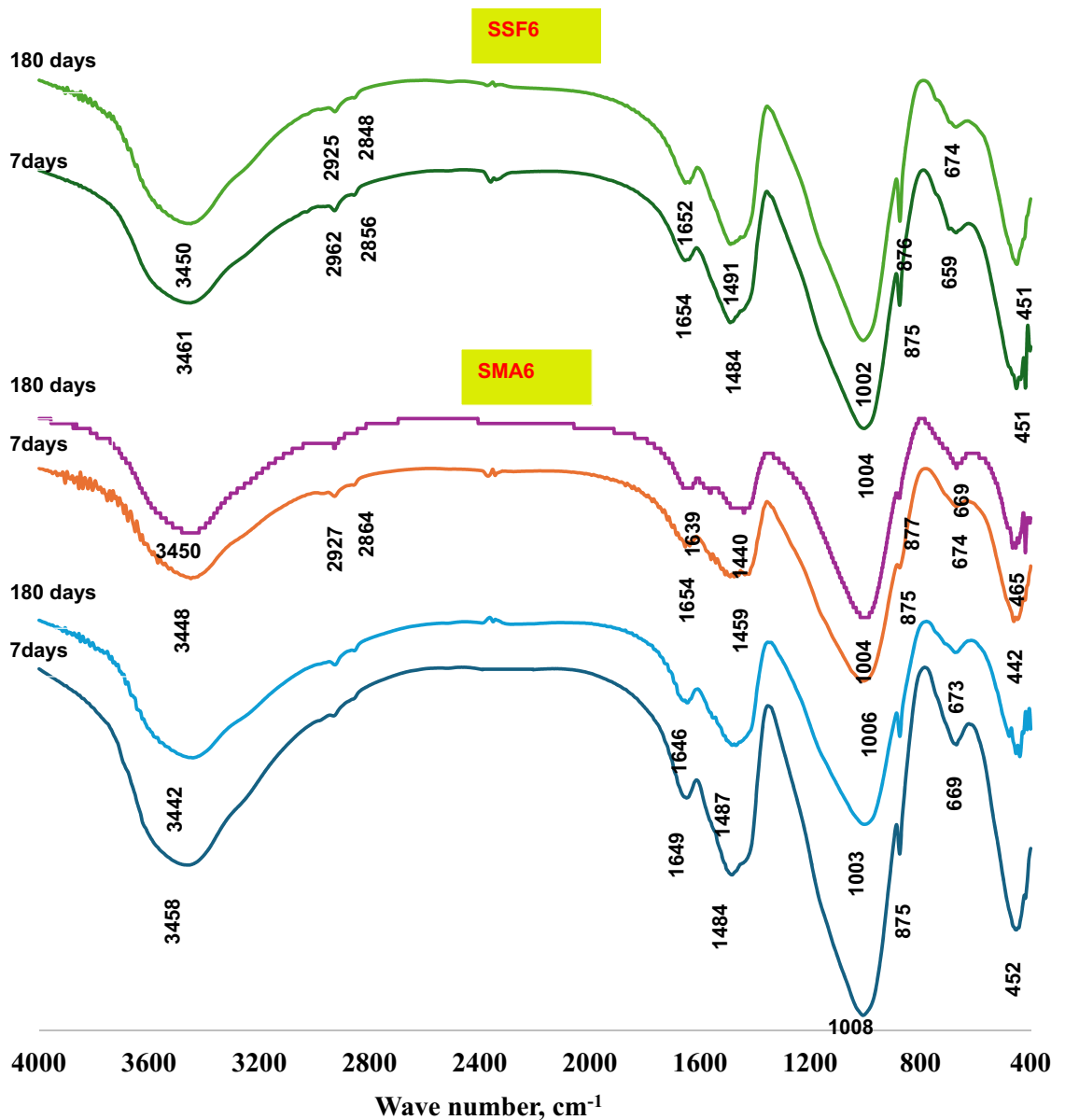


Fig. 5. FTIR-spectra of the geopolymer at 7 days and 180 days.

intensity of the amorphous CSH hump becomes more pronounced over time, suggesting a more developed and homogeneous geopolymeric gel. Moreover, The NASH and CASH peaks become more prominent at 180 days. Generally, the increase in the amorphous phases and the reduction in unreacted precursor materials correlate with an increase in compressive strength. Furthermore, both SMA and SSF show a decrease in intensity of the hydration product characteristic peaks (CSH, CASH), indicating that the slag particles may be coated with MLA and Styrofoam, which would prevent the slag from geopolymerizing. This was coherent with the results of compressive strength.

SEM analysis

In general, the microstructure of the geopolymeric matrix and the shape of the created binding phases have a major impact on the mechanical performance. The SEM micrographic images of the S, SMA6, and SSF6 after 7 days of hydration are demonstrated in Fig. 7. The presence of crosslinked fibers C-S-H is visible in micrographic pictures, which have greater filling ability, providing evidence for the development in the compressive-strength value and presenting a much denser matrix⁴⁵. In mix S, a more uniform and smoother surface is a result of the particles' denser packing, in particular. However, there is a different surface characteristic, with large interparticle gaps and uneven surfaces, in mix SMA6% and SSF6%. According to these findings, adding MLA and Styrofoam to the geopolymer matrix increases its porosity and surface roughness. Greater surface roughness and porosity both lead to a larger surface area. The BET study provides more evidence for these structural alterations⁴⁶.

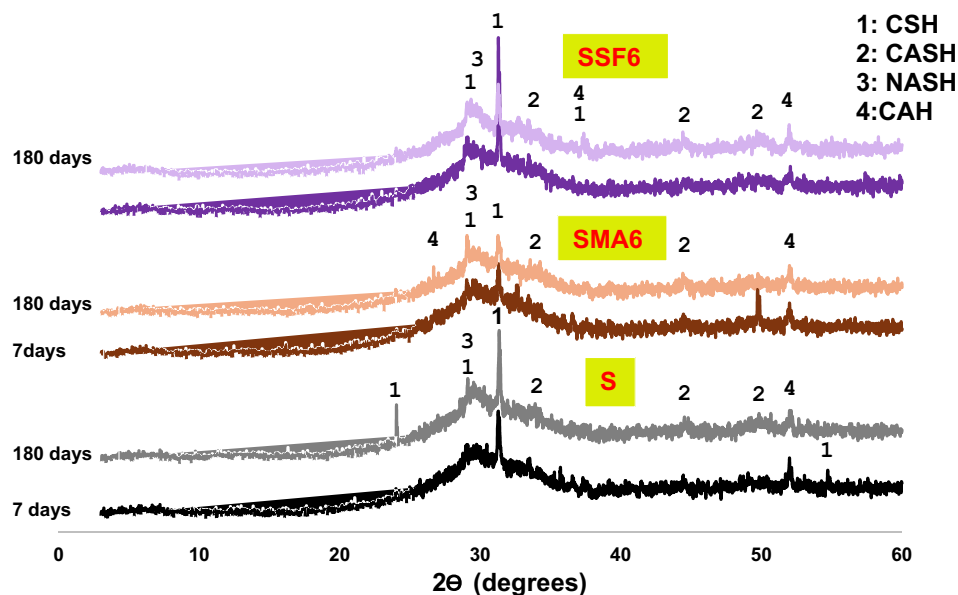


Fig. 6. XRD of the geopolymer at 7 and 180 days.

Moreover, SEM analysis of the samples revealed the emergence of several microcracks on the specimens' surfaces, and SSF6 shows more cracks with a larger pore size (Table 3). This cracking is primarily caused by uneven shrinkage within the geopolymer matrix or by fast water loss via evaporation during the hardening phase^{47,48}. This observation was consistent with the XRD and mechanical properties results, which confirm the lower mechanical properties of SMA6 and SSF6 than the reference mix (S). Furthermore, SSF6 shows the creation of interweaved fibers from C-S-H and a zeolite structure shaped like a flower. These findings are allied to the results reported in a recent study⁴⁹.

Texture characteristics of the prepared geopolymers

The texture characteristics greatly help us explain the adsorption performance of the prepared geopolymers, using the N_2 -adsorption/desorption technique. BET models were used to determine important parameters like average pore diameter, specific surface area, and total pore volume. The BJH model was used to determine the types of pores (micro, meso, or macro). Moreover, isotherm types of geopolymer samples were categorized using IUPAC guidelines to detect the adsorption performance of the prepared geopolymeric composites⁵⁰. The BET pore diameter, pore volume, and surface area are shown in Table 3. According to the data, the control mix's (S) specific surface area, pore volume, and pore diameter are, respectively, 11.277 m^2/g , 0.034 cm^3/g , and 6.023 nm (Table 3). These findings suggest that Mix S possesses an H3 hysteresis loop and a mesoporous structure (Fig. 8). Following modification, the BET surface area, pore volume, and pore diameter for SMA6 and SSF6 (Table 3) changed to 17.524 m^2/g , 0.050 cm^3/g , 5.759 nm, and 53.179 m^2/g , 0.079 cm^3/g , 3.004 nm, respectively. Additionally, the SMA6 and SSF6 adsorbents fit more closely to a type IV isotherm than to a type VI isotherm and exhibit a mesoporous shape. The rougher structure seen in SEM micrographs and the larger surface area offer additional CV binding active sites, enhancing the material's ability to adsorb and remove CV⁵¹.

Adsorption investigations

Effect of pH

The point of zero charge (pHpzc) is crucial for understanding how geopolymer adsorbents interact with crystal violet (CV) dye⁵². It dictates the geopolymer's surface charge and, consequently, its ability to remove CV ions. To ensure effective adsorption, a pH range of 2–8 was used. While factors like chemical composition and curing conditions influence the pHpzc, adding MLA and SF had little effect on the pHpzc in the studied geopolymers, which was estimated to be around 8 as shown in Fig. 9 and Table 4. It was observed that the adsorption capacity (Fig. 10) and removal efficiency (Table 5) increase as the pH increases up to 8. Consequently, the geopolymer surface becomes positively charged when the pH of the solution falls below the pHpzc, which results in electrostatic repulsion with the positively charged CV ions and decreased adsorption^{53,54}. Conversely, at pH values close to the pHpzc, the surface gains a negative charge, which significantly enhances electrostatic attraction and thus improves adsorption performance. This finding allies with the results of other investigations that have been published in the literature^{55–60}.

Effect of adsorbent dose

The amount of adsorbent used has a significant impact on the material's adsorbent capacity. To improve adsorption performance, the adsorbent dosage was optimized, as shown in Fig. 11. Overall, the adsorption efficiency increases as the dosage of geopolymer composite increases from 0.01 g to 0.2 g (see Table 5). This is because higher doses increase the number of adsorption-active sites, increasing the probability of crystal violet

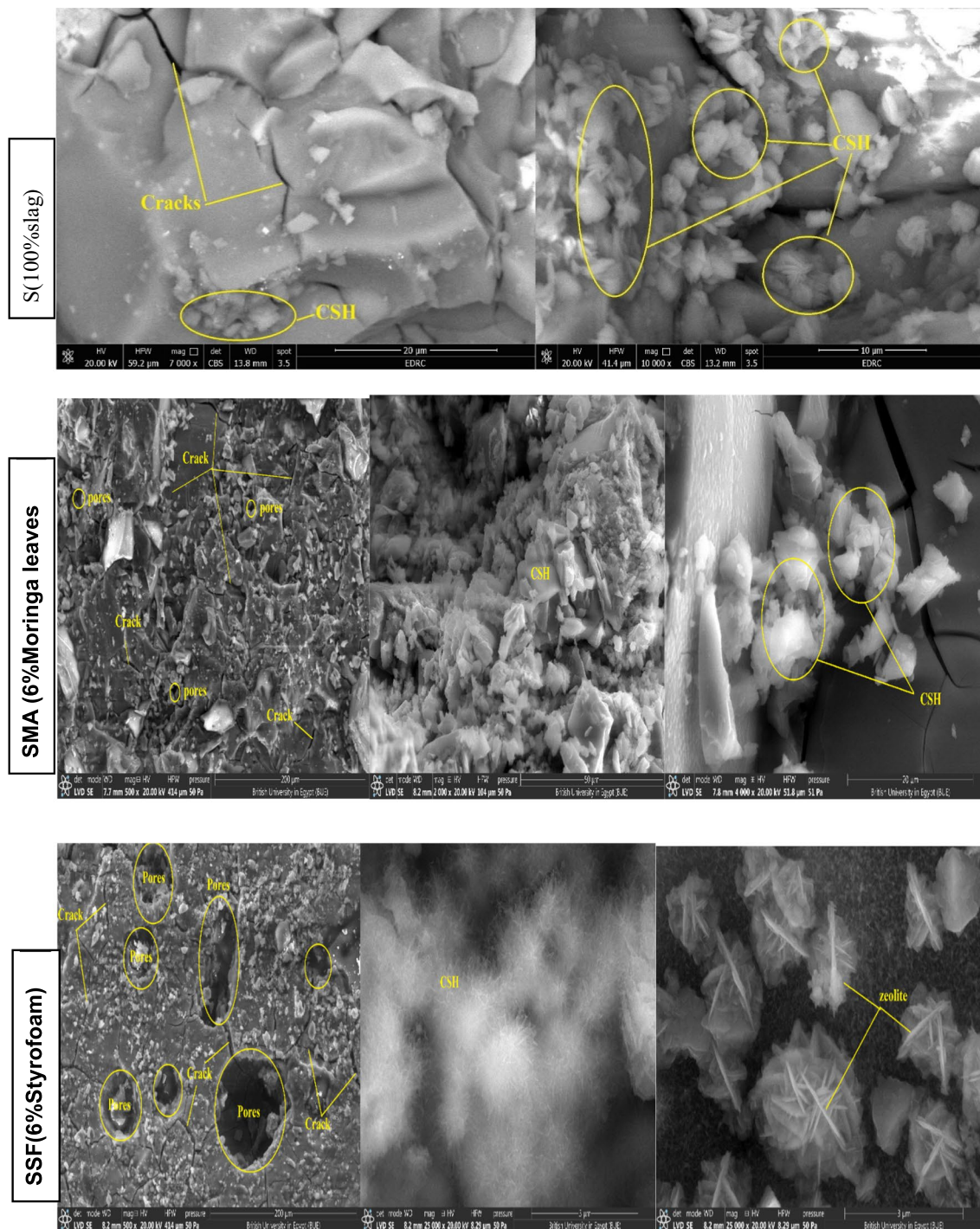


Fig. 7. SEM micrographs of hardened geopolymers after 7 days of hydration at different magnifications.

Adsorbent	SBET, m ² .g ⁻¹	Pore volume, cc.g ⁻¹	Average pore radius, nm
S	11.27	0.03	6.02
SMA6	17.52	0.05	5.76
SSF6	53.18	0.08	3.00

Table 3. The main pore structure analysis characteristics parameter.

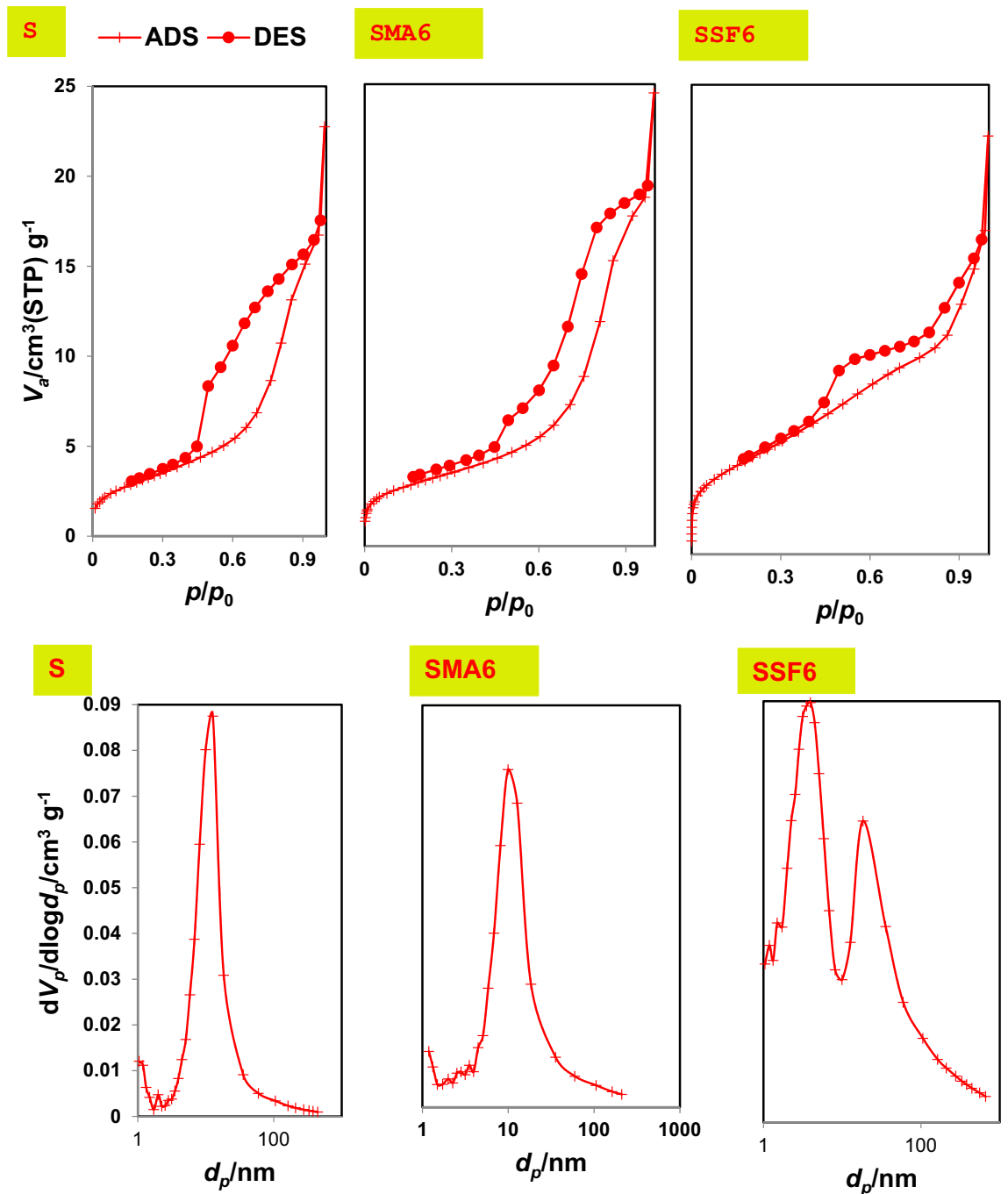


Fig. 8. N_2 -adsorption/desorption isotherm and BJH-pore size distribution for all mixes, respectively.

interacting with the geopolymer material. However, the adsorption capacity decreases with doses above 0.01 g, as the adsorbent particles aggregate and the adsorption sites become saturated, reducing the available surface area for adsorption⁵⁹. The following studies were conducted using the ideal adsorbent dosage of 0.01 g.

Effect of contact time

In this investigation, we investigated how contact time affects the adsorption of CV dye on geopolymer composite samples at room temperature. Our findings, as illustrated in Fig. 12 and Table 5, revealed that the majority of the dye was absorbed during the adsorption's initial half-hour process across all geopolymer samples, albeit with variations in adsorption capacity. The existence of accessible adsorption sites at the beginning stage is responsible for this quick adsorption. After reaching equilibrium and saturating the accessible sites, no further adsorption occurred⁵⁹. Efficiency decreases as the active sites on the geo-adsorbents get saturated, resulting in a lower adsorption rate due to fewer accessible sites for absorbing new dye ions.

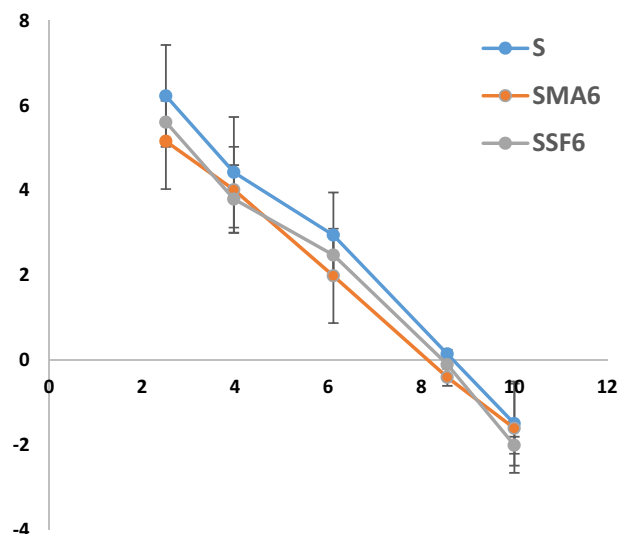


Fig. 9. The point of zero charge of various prepared geopolymer composites.

Geopolymer mix	S	SMA6	SSF6
PZC	8.70	8.20	8.50

Table 4. The point of zero charge of various prepared geopolymer composites.

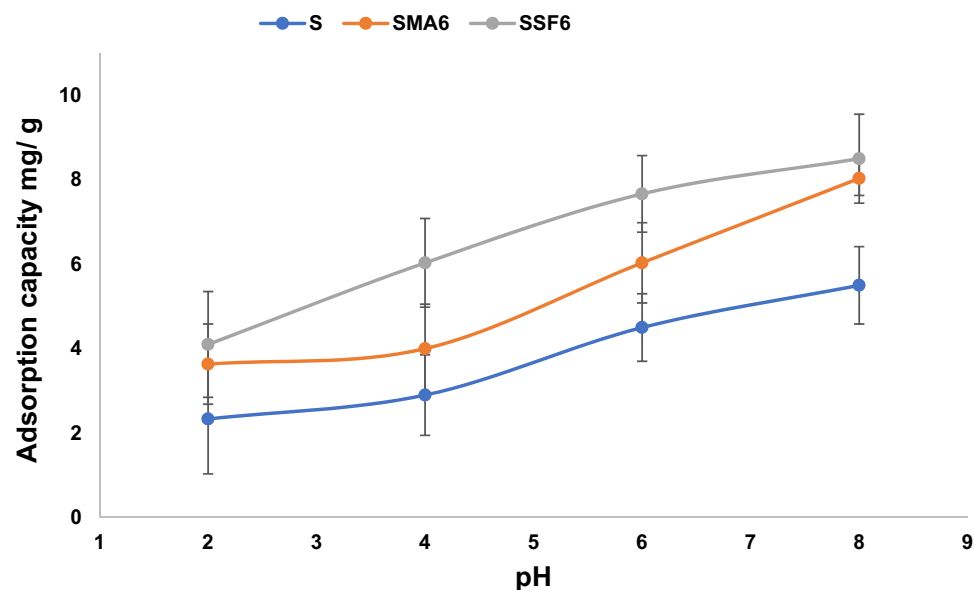


Fig. 10. Effect of pH on CV adsorption capacity (Time 60 min, weight of adsorbent 0.05 g, concentration of dye 10 mg/L).

Effect of dye concentration

The adsorption capacity and removal efficacy at several initial dye concentrations are shown in Fig. 13 and Table 5. Different concentrations of CV were utilized to assess the influence of the initial dye concentration (ranging from 10 mg/L to 120 mg/L) on removal efficiency. The removal efficiency increases alongside the adsorbent's loading capacity as the initial dye concentration rises, until the number of active sites that can bind with dye molecules is exhausted⁵². A similar study on the effects of these parameters on CV adsorption revealed a similar trend^{52,56}. Based on the result, the adsorption capacity and removal efficiency of Styrofoam slag-based

		S	SMA6	SSF6
pH	2	24.63	36.20	40.20
	4	29.11	40.11	60.30
	6	45.60	60.11	77.60
	8	57.42	77.07	85.98
Dose	0.01	58.59	74.31	77.52
	0.05	65.42	77.07	85.98
	0.07	69.35	78.14	89.66
	0.1	68.92	79.22	91.21
	0.15	72.10	82.54	93.59
	0.2	73.23	84.68	95.05
Time (min.)	30	52.69	74.32	77.73
	60	50.59	74.31	77.52
	120	46.95	74.14	75.15
	180	46.50	73.31	74.52
	240	46.01	72.31	74.15
	300	45.95	72.14	73.51
	360	45.95	71.31	73.15
Concentration (mg/l)	10	52.69	77.62	77.73
	30	38.14	67.73	70.73
	60	29.17	62.00	64.00
	80	25.56	63.43	63.73
	100	22.00	58.83	62.13
	120	20.90	57.53	60.73

Table 5. Removal efficiency values of various prepared geopolymer composites.

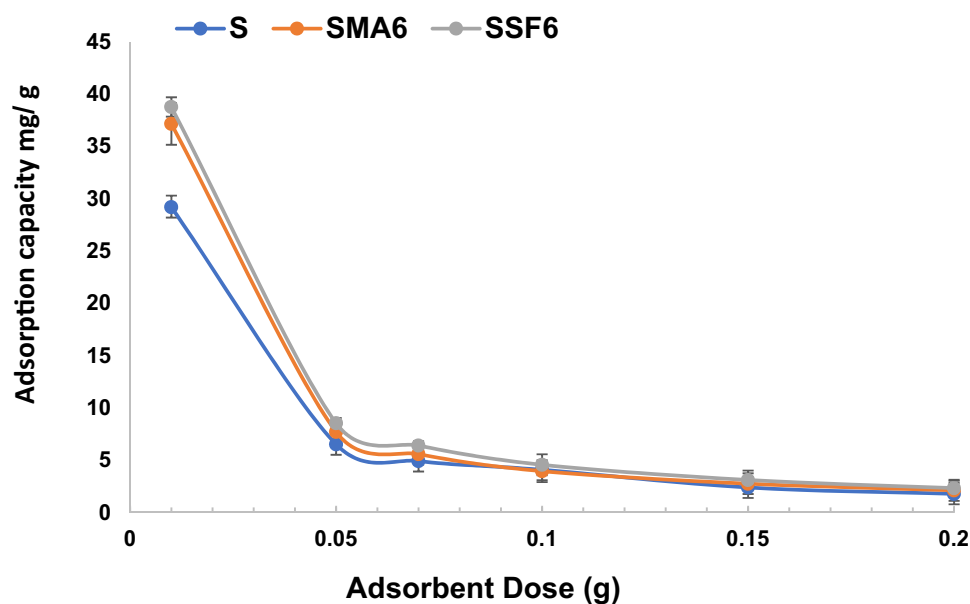


Fig. 11. Effect of adsorbent weight on CV adsorption capacity (Time 60 min, pH 8, concentration of dye 10 mg/L).

geopolymer composite are higher than moringa leaves ash composite and reference mix, which conforms to the porous structure and higher surface area of SSF6, which is sufficient to adsorb more CV.

Adsorption isotherm

An isotherm for adsorption is essential to elucidate how CV interacts with the various prepared geopolymer composites. Freundlich multi-layer and Langmuir single-layer models were employed to model the equilibrium data for CV adsorption. The Langmuir adsorption model effectively describes single-layer adsorption and is

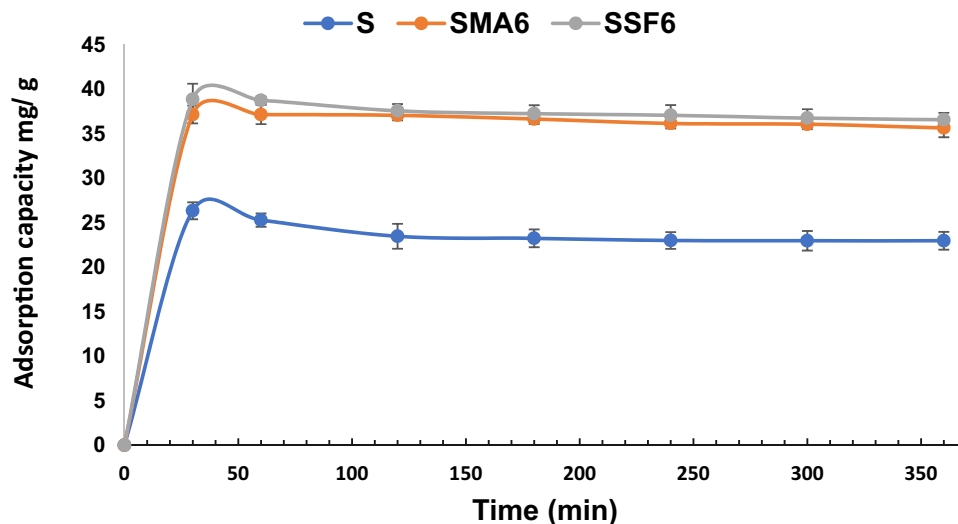


Fig. 12. Effect of time on CV adsorption capacity (pH 8, weight of adsorbent 0.01 g, concentration of dye 10 mg/L).

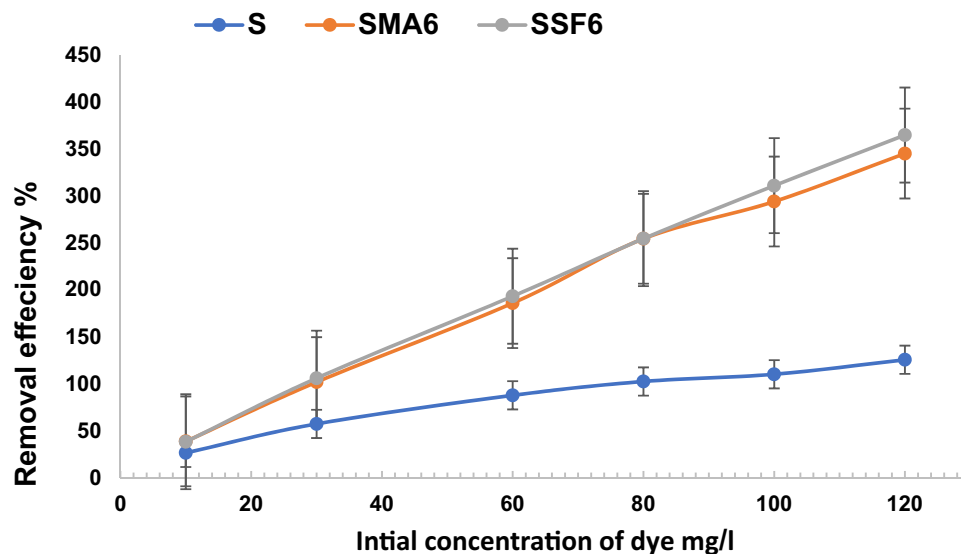


Fig. 13. Effect of initial concentration on CV adsorption capacity (Time 60 min, weight of adsorbent 0.01 g, pH8).

predicated Based on the idea that adsorption takes place on a uniform surface of the adsorbent. Furthermore, adsorbed molecules remain stationary, and all surface sites are equivalent^{59,60}. The data collected between 10 and 120 ppm were fitted to the Langmuir adsorption model, as illustrated in Fig. 14, with correlation coefficients (R^2) of 0.993, 0.9882, and 0.9989 for S, SMA6, and SFF6, respectively. Table 6 shows K_p , R_p , and q_{max} for the geopolymer mixes. The geopolymer's adsorption of CV has R_l values of (0.656, 0.664, and 0.696) for S, SMA6, and SFF6, respectively, indicating a favorable adsorption process. The q_{max} (434.782 mg/g) confirms the improved adsorption performance of SSF. The equilibrium data were subsequently considered utilizing the Freundlich isotherm model, which demonstrated a mechanism of heterogeneous adsorption by plotting $\log q_e$ vs. $\log C_e$, as shown in Fig. 14. The Freundlich multi-layer adsorption model describes heterogeneous systems with non-uniform adsorption sites, in contrast to the Langmuir isotherm. The correlation coefficient value ($R^2 = 0.996, 0.9963, 0.9942$ for S, SMA6, and SFF6, respectively) of the Freundlich model best matched the experimental results of CV adsorption on the geopolymer composite. Consistent with the outcomes regarding the R_l value, the results indicated that n has a value greater than unity, suggesting that the adsorption process of CV dye is advantageous for the produced geopolymer. A high value of the Freundlich constant (k_f) implies that CV can be readily absorbed from an aqueous solution, as shown in Table 6. The results demonstrated that this adsorption interaction process supported the Freundlich theory for geopolymer mixes.

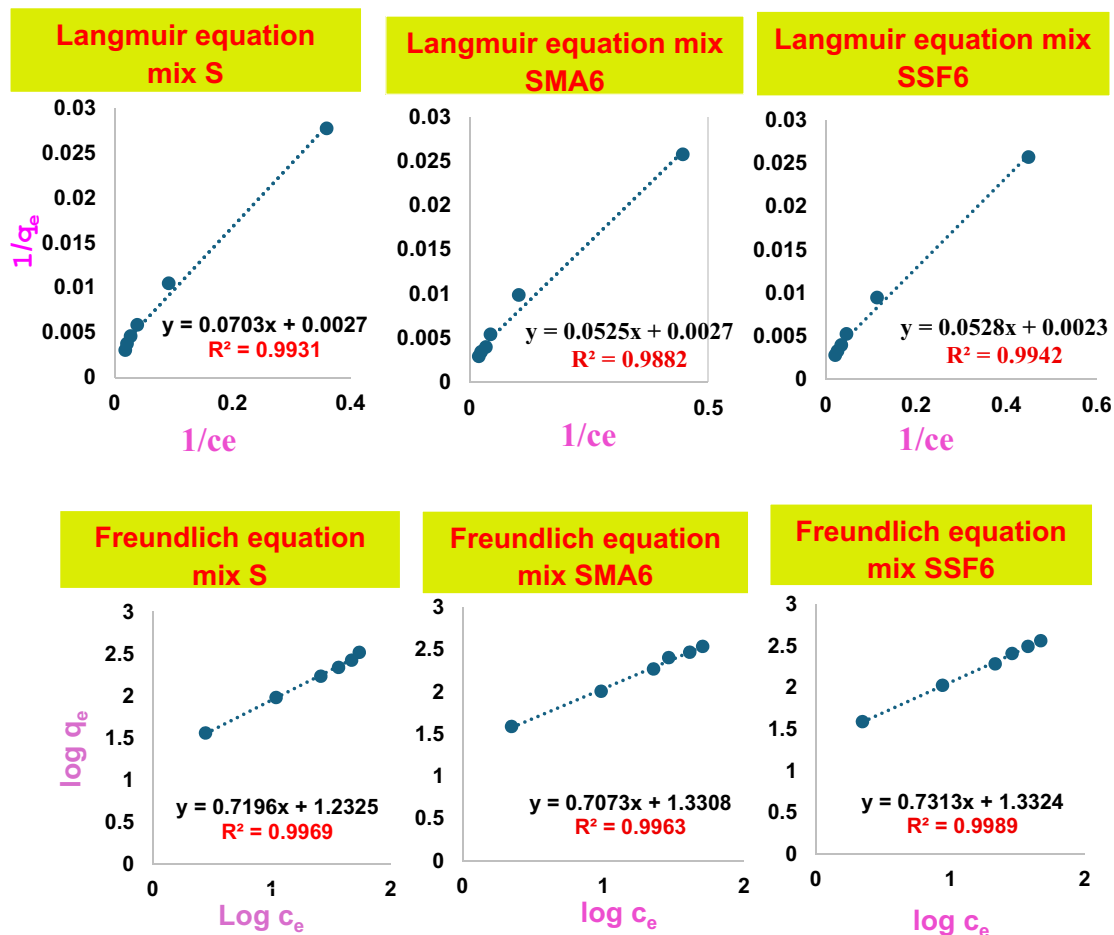


Fig. 14. The fitting results of Langmuir model and Freundlich model.

Isotherm parameter				
Type of isotherm	Parameters	S	SMA6	SSF6
Langmuir	q_{max} (mg/g)	131.58	370.37	434.78
	k_L (L/mg)	0.05	0.05	0.04
	R_L	0.66	0.66	0.70
	R^2	0.993	0.9882	0.9989
Freundlich	K_F	12.20	21.42	21.50
	n	0.52	1.41	1.37
	R^2	0.996	0.9963	0.9942

Table 6. Isotherm parameters for the adsorption behavior of various modified geopolymer cement mixes towards crystal Violet dye.

Adsorption kinetics

It is crucial to understand the process and rate of CV adsorption onto geopolymer composites, as the system's kinetics significantly influences the removal performance. The correlation coefficients and kinetic parameters for CV's adsorption onto geopolymer composites are illustrated in Fig. 15; Table 7. The correlation coefficient (R^2) was used to show the consistency of the model and data. Findings showed that the pseudo-first-order kinetic model has a significantly lower correlation coefficient than the pseudo-second-order kinetic model. Additionally, the q_e value obtained from the fitted linear plot of the pseudo-second-order model aligns more closely with the experimental data in contrast to the pseudo-first-order model. These findings demonstrated that the adsorption is irreversible and that the rate-determining phase is accomplished by chemisorption^{61,62}. It can be attributed to the surface complexation reaction between the negative charges on the geopolymer created by the deprotonation of silanols (SiO-H) and aluminol (AlO-H) groups present and the CV (cationic species) that predominate in a water-soluble solution at the used pH = 8⁵⁶. Comparable kinetic results were reported for the

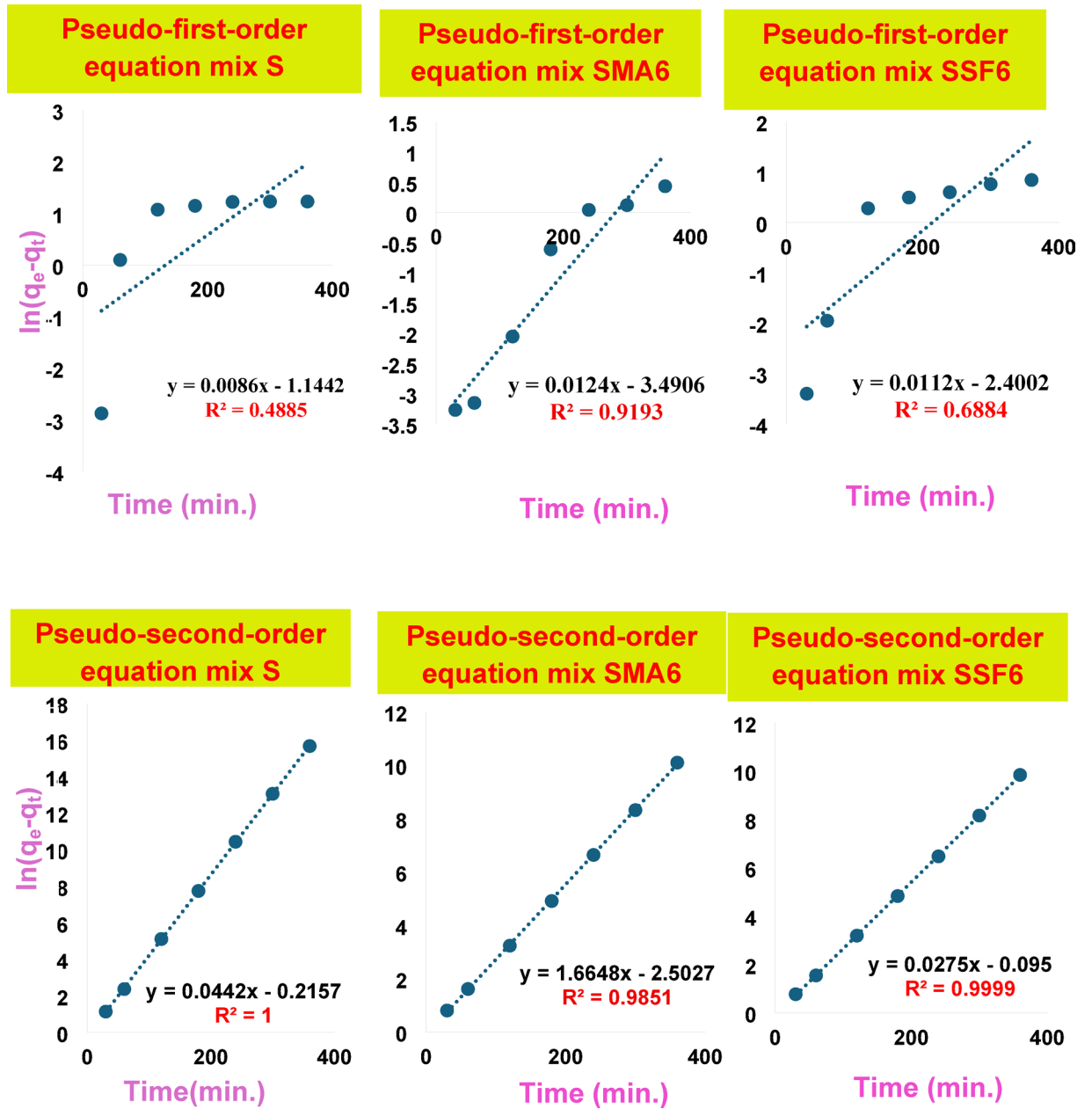


Fig. 15. The fitting results of the pseudo-first-order and pseudo-second-order equations.

Kinetic parameter				
Type of model	Parameters	S	SMA6	SSF6
Pseudo-first-order	q_e (mg/g)	0.003	0.077	0.090
	K_1 (L/mg)	0.00007	0.00002	0.00003
	R^2	0.3625	0.9318	0.6884
Pseudo-second-order	q_e	22.62	34.01	36.36
	K_2	-0.005	-0.0076	-0.0081
	R^2	1	0.9998	0.9999

Table 7. Kinetic parameters for the adsorption behavior of various modified geopolymer cement mixes towards crystal violet dye.

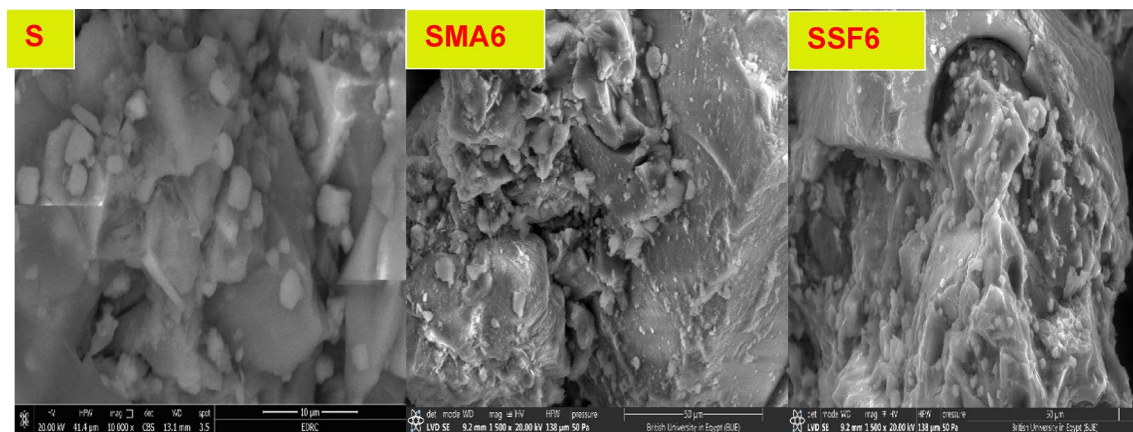


Fig. 16. SEM micrographs of geopolymer after adsorption of CV.

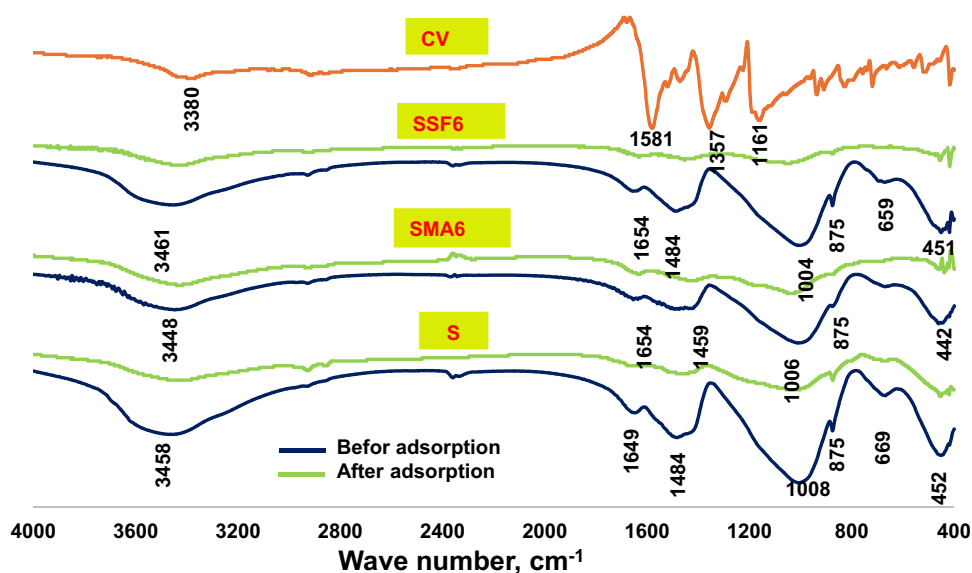


Fig. 17. FTIR-spectra of the geopolymer before and after adsorption of CV.

adsorption of CV onto different adsorbent^{55,56,62}. In summary, the great fit of the pseudo-second-order model indicates the main element controlling the adsorption of CV is chemical interactions onto geopolymer materials. Multiple phases are also included in the adsorption mechanism, and the increased porosity of SSF geopolymers greatly enhances intra-particle diffusion.

Microstructure of geopolymer composites after the adsorption of crystal violet dye

The SEM micrographic images of the S, SMA6, and SSF6 after CV adsorption are presented in Fig. 16. It is observed that the surface roughness of the geopolymer particles is somewhat modified, characterized by the adherence of CV to their surfaces. Furthermore, the surface becomes more uniform and less porous as CV molecules fill the cracks, causing them to vanish, indicating that CV dye molecules have been successfully fixed on the surface of the geopolymer⁶³.

The crystal violet FTIR spectra and the slag geopolymer composites spectra before and upon adsorption are shown in Fig. 17. Crystal violet exhibits bands linked to its functional groups: an aromatic C–H stretching band around 3000 cm^{-1} , an aromatic C=C stretching band in the range of 1500–1600 cm^{-1} . The band around 2915 cm^{-1} refers to $\text{CH}_3\text{-N}$ group characterized by C–N stretching band between 1200 and 1350 cm^{-1} ¹⁶⁴. A phenolic O–H stretching band around 3300 cm^{-1} ¹⁶⁵. Comparing the bands before and after adsorption, the wide O–H stretching band moved to about 3330 cm^{-1} , which also shows a decrease in intensity, demonstrating the presence of hydrogen bonds between CV and the hydroxyl groups on the geopolymer surface. The reduction in Si–O–T stretching asymmetric vibration bands can also be observed. This suggests that CV may have interacted with the geopolymeric silicate network through electrostatic attraction⁶⁶. The small decrease in minor peaks,

like the Si-O/Al-O bending bands, further suggests that the insertion of CV has caused subtle modifications in the framework.

Adsorption mechanism of crystal violet on geopolymer composites

The process by which CV dye adheres to geopolymer composites involves a combination of physisorption and chemisorption mechanisms. While the initial dye uptake is largely driven by electrostatic and van der Waals forces, the strong retention of CV molecules is attributed to chemisorption through hydrogen bonding, ionic interactions, and complexation with the geopolymer matrix⁶⁷. Understanding these mechanisms helps in designing more effective adsorbents and optimizing their performance for wastewater treatment applications.

The key factors contributing to physisorption in this system include⁶⁸:

Porous structure contribution Geopolymers typically exhibit micro- and mesoporous structures, which enhance dye uptake by providing a large surface area for adsorption, as confirmed by BET/BJH analyses.

Electrostatic interactions At pH 8, the positively charged CV molecules adhere to the negatively charged geopolymer surface, resulting in strong electrostatic adsorption.

The main chemisorption mechanisms in this system include^{67,69}:

Hydrogen bonding Hydrogen bonds are formed between the hydroxyl groups (OH⁻) in the geopolymer structure and the nitrogen atoms (N⁺) in the CV molecules.

Ionic interactions The pseudo-second-order kinetic model suggests that chemisorption plays a dominant role, as electron exchange occurs linking the functional groups of CV and the geopolymer surface.

Complexation with active sites The geopolymer matrix contains Si-O and Al-O functional groups that can participate in electron sharing or exchange interactions, forming stable bonds with dye molecules.

Figure 18 shows the Schematic diagram of the proposed adsorption mechanism.

Comparative analysis with adsorbents from other research studies

Table 8 presents a comparative analysis of the synthesized geopolymers' crystal violet dye adsorption capacity against other adsorbents documented in prior research. Comparatively, different adsorbents exhibit varying levels of efficiency (Table 8). A maximum capacity of 454.5 mg/g for CV dye is demonstrated by ball milled royal palm leaf sheath powder at a dosage of 40 mg/L, initial concentration of 100 mg/L, contact period of 60 min, pH 6, and 30 °C. However, the minimum adsorption capacity (14.66 mg/g) is given by acid-activated volcanic ash/rice husk based geopolymer at dose of 0.2 g, pH 6, 60 g/l dye concentration and 60 min. While earlier studies have thoroughly examined adsorbents derived from various industrial and agricultural by-products, the geopolymers developed in this study exhibit competitive performance, achieving a maximum adsorption capacity of 434.7 mg/g for SSF6. This enhanced capacity is attributed to the synergistic effect of incorporating Styrofoam (SF) and moringa leaf ash (MLA), which increased the specific surface area of SSF6 and SMA to 53 and 17.50 m²/g, thereby providing more active sites for crystal violet adsorption. The improved performance of geopolymers made from Styrofoam and moringa leaf ash positions them as highly effective dye adsorbents. Additionally, these materials contribute to the creation of sustainable construction products by utilizing waste

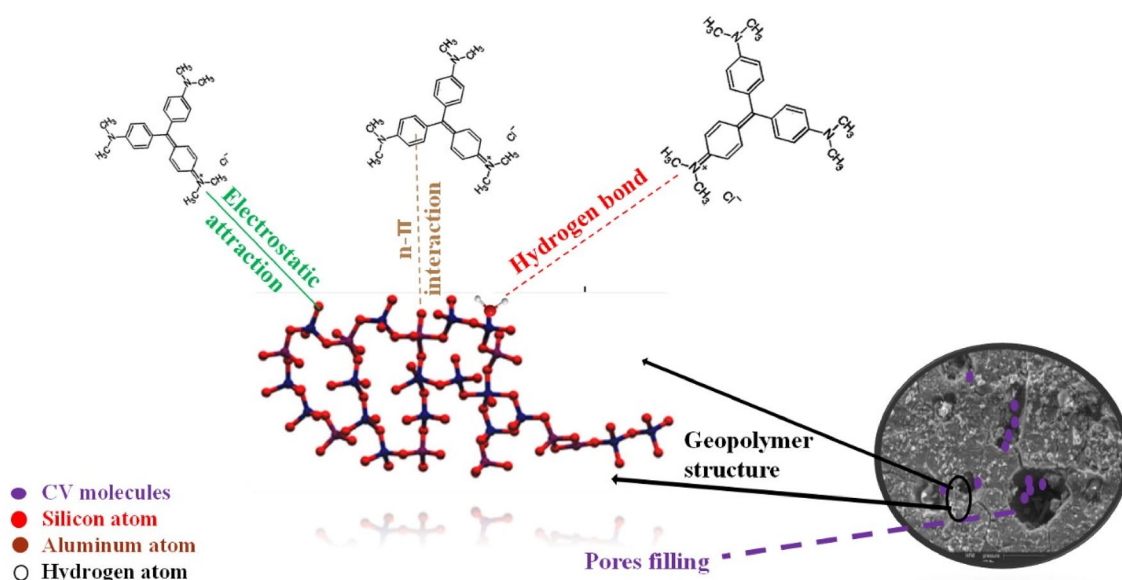


Fig. 18. Schematic diagram of the proposed adsorption mechanism.

Adsorbent	Form	Maximum capacity (mg/g)	Operational condition					Reference
			Dose	Time	Initial concentration	pH	Temperature	
Banana stem biochar (Pyrolyzed at 350 °C)	Powder	208.33	25 mg	60 min.	100 g/L	3 pH	25 °C	73
The acid-activated volcanic ash/rice husk ash-based geopolymer (GPa)	Powder	14.66	0.2 g	60 min.	60 g/L	6 pH	25 °C	74
Mesoporous geopolymer using metakaolin and rice husk ash	Powder	276.9	1.5 g/l	120	50 mg/L	4.5 pH	54.85 °C	75
Royal palm leaf sheath powder	Powder	344.83	40 mg	60 min.	100 g/L	6 pH	30 °C	76
Ball milled Royal palm leaf sheath powder	Powder	454.5	40 mg	60 min.	100 g/L	6 pH	30 °C	76
Optimized geopolymer (GPO)	Powder	69.19	1.5 g/L	120	20–140 mg/L	6.5 pH	20 °C	77
Vermiculite based geopolymer	Powder	29.6	0.3 g	15 min.	30 g/L	8 pH	30 °C	28
Moringa seeds powder slag based geopolymer (SM3)	Powder	322.58	0.01 g	30 min.	120 g/L	8 pH	25 °C	26
MLA6	Powder	370.370	0.01 g	30 min.	120 g/L	8 pH	25 °C	Present study
SSF6	Powder	434.782	0.01 g	30 min.	120 g/L	8 pH	25 °C	Present study

Table 8. Comparison between adsorption values for CV by using different adsorbents.

by-products. This use of waste materials not only helps reduce the amount of refuse sent to landfills but also promotes environmental sustainability. The development of these geopolymers showcases the potential for innovative solutions that address both environmental and industrial challenges.

Limitations of our study

Slag-based geopolymer composites incorporating Styrofoam and Moringa Leaf Ash present in this study a promising approach to sustainable wastewater treatment for removing Crystal Violet dye, promoting circular economy principles using agricultural and industrial wastes. However, evaluating the geopolymer's ability to regenerate and be reused remains a significant challenge. Recovering and further treatment techniques are needed to regenerate geopolymer materials after dye adsorption, as noted in previous studies^{70–72}. The long-term effectiveness of the geopolymer as an adsorbent may be reduced if the dye adsorption process causes structural and chemical changes in the material^{70–72}. This highlights the urgent need for effective and affordable regeneration techniques. Current regeneration methods are often complicated, resource-consuming, and may weaken long-term performance^{70–72}. Developing efficient and cost-effective regeneration solutions is critical to preserving adsorption capacity and structural integrity through multiple cycles^{70–72}. Further research is essential to create such techniques, with careful attention to the environmental impact of the regeneration process to ensure true sustainability.

Our future research will focus on improving the specific surface area of geopolymers and developing effective regeneration methods. By increasing the surface area, we aim to enhance adsorption capacity and dye removal efficiency, possibly using pore-forming agents or optimizing synthesis processes. Additionally, creating robust regeneration techniques is essential. We will explore innovative approaches to reduce the use of harsh chemicals and energy-consuming methods, such as thermal treatment. Our ultimate goal is to develop sustainable regeneration strategies. This will help lower the environmental impact of the process and support the overall sustainability of the dye removal system. By prioritizing both efficiency and eco-friendliness, we intend to establish new standards for regeneration techniques in water treatment.

Conclusions

This research explores using industrial waste (ground granulated blast-furnace slag and Styrofoam) and agricultural waste (Moringa leaf ash) to create geopolymer cement. The goal is to develop a material with strong mechanical properties and the ability to absorb harmful dyes, like crystal violet, from wastewater. The study produced two geopolymer composites, each incorporating either Styrofoam or Moringa leaf ash, aiming to provide both economic and environmental advantages. This work advances sustainable construction and wastewater treatment solutions.

- The incorporation of MLA and Styrofoam generally reduces compressive strength and increases porosity in geopolymeric composites but still have mechanical integrity.
- Nitrogen adsorption and desorption analyses for the prepared geopolymer composites near to Type IV than Type VI isotherms with H3 hysteresis, indicating the existence of mesoporous structures. Notably, the SSF6 geopolymer composite, characterized by its fine mesoporous structure and the highest surface area, exhibited a significantly enhanced adsorption capacity compared to the control mix (S).
- In adsorption performance, the most successful sample was determined to be the SSF6 geopolymer. The SSF6 geopolymer showed a maximum CV capacity of 434.782 mg/g, under ideal circumstances (pH 8, contact period of 30 min, adsorbent dosage of 0.01 g L⁻¹, and beginning dye concentration of 10 mg L⁻¹).
- The adsorption mechanism demonstrated multilayer chemisorption by adhering to the Freundlich isotherm and pseudo-second-order kinetic model.
- The adsorption of crystal violet dye onto geopolymer composites is influenced by both physisorption and chemisorption. Initial adsorption is driven by the porous structure of the geopolymer and electrostatic in-

teractions, while stronger retention occurs through hydrogen bonding, ionic interactions, and complexation between the dye and the geopolymer matrix.

From our study findings, incorporating industrial and agricultural waste into geopolymer composites has improved their adsorption behavior. This enhancement increases their effectiveness in environmental applications, particularly in wastewater treatment. Additionally, recycling industrial and agricultural waste to produce new building materials serves a dual purpose, benefiting both environmental sustainability and the construction industry. Future research should concentrate on pilot-scale testing, investigate more diverse pollutant types, and evaluate substitute waste-derived activators in order to improve sustainability and lower manufacturing costs. Large-scale viability should also be assessed using life cycle and techno-economic analyses.

Data availability

The authors declare that the data supporting the findings of this study are available within the paper. Should any raw data files be needed in another format, they are available from the corresponding author upon reasonable request. Source data are provided with this paper.

Received: 2 June 2025; Accepted: 12 September 2025

Published online: 07 October 2025

References

- Orhan, T. Y., Karakoç, M. B. & Özcan, A. Durability characteristics of slag based geopolymer concrete modified with crumb rubber. *Constr. Build. Mater.* **404**, 132851. <https://doi.org/10.1016/j.conbuildmat.2023.132851> (2023).
- Davidovits, J. Application of Ca-Based geopolymer with blast furnace slag, a review. <https://www.researchgate.net/publication/268337141> (2011).
- Guzel, G. & Deveci, H. Properties of polymer composites based on bisphenol A epoxy resins with original/modified steel slag. *Polym. Compos.* **39**, 513–521. <https://doi.org/10.1002/pc.23962> (2018).
- Maul, J. et al. Polystyrene and styrene copolymers. In *Ullmann's Encyclopedia of Industrial Chemistry* **29**, 475–522. https://doi.org/10.1002/14356007.a21_615.pub2 (2007).
- Chandra, M., Kohn, C., Pawlitz, J. & Powell, G. Real cost of styrofoam. *Saint Louis Univ. MGT* 6006–6002 (2016).
- Ming, Y., Wenyun, S., Yan, Q. & Yujing, N. Study on recycling of waste styrofoam for adhesive. *Advanced Mater. Res.* **181–182**, 975–978 (2011). <https://doi.org/10.4028/www.scientific.net/AMR.181-182.975>
- Osemeahon, S. A., Reuben, U. & Emmanuel, E. Development of adhesive from polystyrene waste. *BIOMED. Nat. Appl. Sci.* **02**, 13–24. <https://doi.org/10.53858/bnas02011324> (2022).
- Zennaki, M. A., Tennouga, L., Bouras, B. & Balkaid, S. Removal of methylene blue dye from an aqueous solution by an adsorption technique using sulfonated polystyrene as three Low-cost adsorbents. *Phys. Chem. Res.* **12**, 453–465. <https://doi.org/10.22036/pcr.2023.400270.2350> (2024).
- Paranje, A. & Kulkarni, P. Experimental investigation on styrofoam based concrete. *Int. J. Mech. Prod. Eng.* **5**, 56–61 (2017).
- Csurhes, S. & Navie, S. Horseradish Tree Moringa Oleifera. (2010).
- Khataee, A., Gholami, P., Vahid, B. & Joo, S. W. Heterogeneous sono-Fenton process using pyrite nanorods prepared by non-thermal plasma for degradation of an anthraquinone dye. *Ultrason. Sonochem.* **32**, 357–370. <https://doi.org/10.1016/j.ultsonch.2016.04.002> (2016).
- Karimi, F. et al. Removal of metal ions using a new magnetic Chitosan nano-bio-adsorbent; A powerful approach in water treatment. *Environ. Res.* **203**, 111753. <https://doi.org/10.1016/j.envres.2021.111753> (2022).
- Al Sharabati, M. et al. Biodegradable polymers and their nano-composites for the removal of endocrine-disrupting chemicals (EDCs) from wastewater: A review. *Environ. Res.* **202**, 111694. <https://doi.org/10.1016/j.envres.2021.111694> (2021).
- Hasan, M. et al. Adsorptive removal of dye from textile wastewater employing *Moringa Oleifera* leaves Biochar as a natural biosorbent. *Biomass Conv Bioref.* **14**, 11075–11091. <https://doi.org/10.1007/s13399-022-03196-4> (2024).
- Mani, S. & Bharagava, R. N. Exposure to crystal violet, its toxic, genotoxic and carcinogenic effects on environment and its degradation and detoxification for environmental safety. In: (ed de Voogt, W.) *Reviews of Environmental Contamination and Toxicology*. **237**. https://doi.org/10.1007/978-3-319-23573-8_4. (Springer, 2016).
- Bharagava, R. N., Mani, S., Mulla, S. I. & Saratale, G. D. Degradation and decolorization potential of a ligninolytic enzyme producing *Aeromonas hydrophila* for crystal Violet dye and its phytotoxicity evaluation. *Ecotoxicol. Environ. Saf.* **156**, 166–175. <https://doi.org/10.1016/j.ecoenv.2018.03.012> (2018).
- C Roy, D. et al. Biodegradation of crystal Violet dye by bacteria isolated from textile industry effluents. *PeerJ* **6** e5015. <https://doi.org/10.7717/peerj.5015> (2018).
- Kolya, H. & Kang, C. W. Toxicity of metal oxides, dyes, and dissolved organic matter in water: implications for the environment and human health. *Toxics* **12**, 111. <https://doi.org/10.3390/toxics12020111> (2024).
- Ogwang, G. et al. Experimental evaluation of rice husk Ash for applications in geopolymer mortars. *J. Bioresources Bioprod.* **6**, 160–167. <https://doi.org/10.1016/j.jobab.2021.02.008> (2021).
- Chen, S., Jiang, S. & Jiang, H. A review on conversion of crayfish-shell derivatives to functional materials and their environmental applications. *J. Bioresources Bioprod.* **5**, 238–247. <https://doi.org/10.1016/j.jobab.2020.10.002> (2020).
- Hosseini Asl, S. M. et al. Porous adsorbents derived from coal fly Ash as cost-effective and environmentally-friendly sources of aluminosilicate for sequestration of aqueous and gaseous pollutants: A review. *J. Clean. Prod.* **208**, 1131–1147. <https://doi.org/10.1016/j.jclepro.2018.10.186> (2019).
- Tan, T. H., Mo, K. H., Ling, T. C. & Lai, S. H. Current development of geopolymer as alternative adsorbent for heavy metal removal. *Environ. Technol. Innov.* **18**, 100684. <https://doi.org/10.1016/j.eti.2020.100684> (2020).
- Zhao, H. Y., Liu, G. L., Huang, Z., Jin, L. Y. & Pei, Y. R. Recent progress of porous geopolymers: nanoporosity regulation toward fundamental applications. *J. Asian. Ceam. Soc.* **12**, 1–13. <https://doi.org/10.1080/21870764.2024.2311458> (2024).
- Sang, M., Zhao, H., Li, Y. & Zhu, L. Preparation of a porous geopolymer (SPG) to be used as an adsorbent for Cu²⁺ Removal. *Langmuir* **40**, 8851–8861. <https://doi.org/10.1021/acs.langmuir.3c04013> (2024).
- Aouan, B. et al. Application of central composite design for optimisation of the development of Metakaolin based geopolymer as adsorbent for water treatment. *Int. J. Environ. Anal. Chem.* **104**, 2623–2641. <https://doi.org/10.1080/03067319.2022.2070010> (2024).
- Hashish, S. A. et al. Development of Moringa seed powder-modified slag geopolymers for enhanced mechanical properties and effective dye removal. *Sci. Rep.* **15**, 9017. <https://doi.org/10.1038/s41598-025-91091-z> (2025).
- Mboka, J. M. et al. Synergistic co-adsorptive removal of crystal Violet and chromium(vi) from water by pozzolan-charcoal based geopolymer composites. *Mater. Adv.* **5**, 6234–6247. <https://doi.org/10.1039/D4MA00408F> (2024).

28. Aouan, B. et al. Development and optimization of geopolymer adsorbent for water treatment: application of mixture design approach. *J. Environ. Manage.* **338**, 117853. <https://doi.org/10.1016/j.jenvman.2023.117853> (2023).
29. Huang, G., Xu, J., Geng, P. & Li, J. Carrier flotation of low-rank coal with polystyrene. *Minerals* **10**, 452. <https://doi.org/10.3390/min10050452> (2020).
30. Islam, M. S., Roy, H. & Afrose, S. Phosphoric acid surface modified Moringa Oleifera leaves Biochar for the sequestration of Methyl orange from aqueous solution: characterizations, isotherm, and kinetics analysis. *Remediation* **32**, 281–298. <https://doi.org/10.1002/rem.21733> (2022).
31. Kumar, A., Saini, K. & Bhaskar, T. Hydrochar and biochar: production, physicochemical properties and techno-economic analysis. *Bioresour. Technol.* **310**, 123442. <https://doi.org/10.1016/j.biortech.2020.123442> (2020).
32. Sahraei Moghadam, A., Mirza Goltabar Roshan, A. & Omidinasab, F. Utilization of agricultural wastes as fiber, binder and aggregates of geopolymer mortars: application of Taguchi method for strength and durability optimization. *J. Building Eng.* **75**, 106906. <https://doi.org/10.1016/j.jobte.2023.106906> (2023).
33. Hoe-Woon, T. et al. Dual-functional geopolymers from industrial and agricultural wastes for copper adsorption and sustainable construction applications. *J. Environ. Chem. Eng.* **13**, 117773. <https://doi.org/10.1016/j.jece.2025.117773> (2025).
34. Ahmed, D. A., El-Asasry, M. A., Aly, A. A. & Ragai, S. M. Green synthesis of the effectively environmentally safe Metakaolin-Based geopolymer for the removal of hazardous industrial wastes using two different methods. *Polym. (Basel)*. **15**, 2865. <https://doi.org/10.3390/polym15132865> (2023).
35. Sayed, M. A. et al. Towards a green climate: production of slag–red brick waste–based geopolymer mingled with WO₃ nanoparticles with bio-mechanical achievements. *Constr. Build. Mater.* **413**, 134909. <https://doi.org/10.1016/j.conbuildmat.2024.134909> (2024).
36. Lei, Z. & Pavia, S. Geopolymer based on biomass Ash from agricultural residues. *Constr. Build. Mater.* **441**, 137471. <https://doi.org/10.1016/j.conbuildmat.2024.137471> (2024).
37. Baziak, A., Plawecka, K., Hager, I., Castel, A. & Korniejenko, K. Development and characterization of lightweight geopolymer composite reinforced with hybrid carbon and steel. *Materials* **14**, 5741. <https://doi.org/10.3390/ma14195741> (2021).
38. Glad, B. E., Han, C. & Kriven, W. M. Polymer adhesion to geopolymer via silane coupling agent additives. *J. Am. Ceram. Soc.* **95**, 3758–3762. <https://doi.org/10.1111/j.1551-2916.2012.05433.x> (2012).
39. Acisli, O., Acar, I. & Khataee, A. Preparation of a fly ash-based geopolymer for removal of a cationic dye: isothermal, kinetic and thermodynamic studies. *J. Ind. Eng. Chem.* **83**, 53–63. <https://doi.org/10.1016/j.jiec.2019.11.012> (2020).
40. Ma, Y. et al. Infrared investigation of organo-montmorillonites prepared from different surfactants. *Spectrochim Acta Mol. Biomol. Spectrosc.* **76**, 122–129. <https://doi.org/10.1016/j.saa.2010.02.038> (2010).
41. Açışlı, Ö., Karaca, S. & Gürses, A. Investigation of the alkyl chain lengths of surfactants on their adsorption by montmorillonite (Mt) from aqueous solutions. *Appl. Clay Sci.* **142**, 90–99. <https://doi.org/10.1016/j.clay.2016.12.009> (2017).
42. Machowska, A. et al. A study of the early hydration processes and properties of fly ash-slag binders. *Bull. Mater. Sci.* **42**, 213. <https://doi.org/10.1007/s12034-019-1886-1> (2019).
43. Lecomte, I. et al. Micro-structural comparison between geopolymers, alkali-activated slag cement and Portland cement. *J. Eur. Ceram. Soc.* **26**, 3789–3797. <https://doi.org/10.1016/j.jeurceramsoc.2005.12.021> (2006).
44. Ramos, F. J. H. T. V., Mendes, L. C. & Cestari, S. P. Organically modified concrete waste with oleic acid. *J. Therm. Anal. Calorim.* **119**, 1895–1904. <https://doi.org/10.1007/s10973-014-4358-2> (2015).
45. Frontera, P., Marchese, S., Crea, F., Aiello, R. & Nagy, J. B. The strength effects of synthetic zeolites on properties of high performance concrete. *WIT Trans. Built Environ. Vol.* **85**, 449–458. <https://doi.org/10.2495/HPSM060441> (2006).
46. Hoe-Woon, T. et al. Assessing viability and leachability in fly Ash geopolymers incorporated with rubber sludge. *J. Ind. Eng. Chem.* **142**, 499–511. <https://doi.org/10.1016/j.jiec.2024.07.057> (2025).
47. Feng, X., Liu, N. & Lu, X. Investigation of un-calcined coal gangue together with ground granulated blast furnace slag and fly Ash to ambient-curing production high-strength geopolymer. *J. Mater. Res. Technol.* **25**, 3985–3997. <https://doi.org/10.1016/j.jmrt.2023.06.249> (2023).
48. Hakem Aziz, I., Mustafa Al Bakri Abdullah, M., Arif Anuar Mohd Salleh, M. & Victor Sandu, A. The incorporation of sodium hydroxide (NaOH) concentration and CaO-Si components on ground granulated blast furnace slag geopolymers. *IOP Conf. Ser. : Mater. Sci. Eng.* **864**, 012005. <https://doi.org/10.1088/1757-899X/864/1/012005> (2020).
49. Chelluri, S. K. & Hossiney, N. Performance evaluation of ternary blended geopolymer binders comprising of slag, fly Ash and brick kiln rice husk Ash. *Case Stud. Constr. Mater.* **20**, e02918. <https://doi.org/10.1016/j.cscm.2024.e02918> (2024).
50. Amin, M. S. et al. Synthesis of multifunctional mesoporous geopolymer under hydrothermal curing: high mechanical resistance and efficient removal of methylene blue from aqueous medium. *Developments Built Environ.* **18**, 100460. <https://doi.org/10.1016/j.dibe.2024.100460> (2024).
51. Chen, Z. et al. Rice husk-based hierarchical porous carbon for high performance supercapacitors: the structure-performance relationship. *Carbon N Y.* **161**, 432–444. <https://doi.org/10.1016/j.carbon.2020.01.088> (2020).
52. Homagai, P. L., Poudel, R., Poudel, S. & Bhattacharai, A. Adsorption and removal of crystal violet dye from aqueous solution by modified rice husk. *Heliyon* **8**, e09261. <https://doi.org/10.1016/j.heliyon.2022.e09261> (2022).
53. Mardenborough, K. et al. Influence of NaOH concentration on the decolorization of crystal Violet dyed cotton fabric. *Environ. Eng. Res.* **28**, 210643. <https://doi.org/10.4491/eer.2021.643> (2023).
54. Potrich, E. & Amaral, L. Determination of kinetic parameters of the crystal Violet reaction with sodium hydroxide applying absorbance technique and the laws of lambert-beer and arrhenius. *Enciclopédia Biosfera.* **14**, 1852–1861. https://doi.org/10.18677/EnciBio_2017A153 (2017).
55. Zamouche, M. et al. Batch mode for adsorption of crystal Violet by Cedar cone forest waste. *SN Appl. Sci.* **2**, 198. <https://doi.org/10.1007/s42452-020-1976-0> (2020).
56. Mittal, A., Mittal, J., Malviya, A., Kaur, D. & Gupta, V. K. Adsorption of hazardous dye crystal Violet from wastewater by waste materials. *J. Colloid Interface Sci.* **343**, 463–473 (2010). <https://doi.org/10.1016/j.jcis.2009.11.060>
57. Chakraborty, S., Chowdhury, S., Saha, P. & Das Adsorption of crystal Violet from aqueous solution onto NaOH-modified rice husk. *Carbohydr. Polym.* **86**, 1533–1541. <https://doi.org/10.1016/j.carbpol.2011.06.058> (2011).
59. Senthilkumaar, S., Kalaamani, P. & Subburaam, C. V. Liquid phase adsorption of crystal Violet onto activated carbons derived from male flowers of coconut tree. *J. Hazard. Mater.* **136**, 800–808. <https://doi.org/10.1016/j.jhazmat.2006.01.045> (2006).
60. Sadoq, M. et al. Elimination of crystal Violet from aqueous solution by adsorption on naturel polysaccharide: kinetic, isotherm, thermodynamic studies and mechanism analysis. *Arab. J. Chem.* **17**, 105453. <https://doi.org/10.1016/j.arabjc.2023.105453> (2024).
61. Abdel Hamid, E. M., Aly, H. M. & El Naggar, K. A. M. Synthesis of nanogeopolymer adsorbent and its application and reusability in the removal of methylene blue from wastewater using response surface methodology (RSM). *Sci. Rep.* **14**, 20631. <https://doi.org/10.1038/s41598-024-70284-y> (2024).
62. El Alouani, M. et al. Application of mesoporous fly Ash as a low-cost adsorbent for effective removal and immobilization of hazardous pollutants in aqueous environments. *Model. Earth Syst. Environ.* **9**, 3539–3552. <https://doi.org/10.1007/s40808-023-01715-4> (2023).
63. Huang, Y. P. et al. Selective adsorption of crystal Violet via hydrogen bonded water bridges by InVO₄. *Chem. Eng. J. Adv.* **15**, 100508. <https://doi.org/10.1016/j.ceja.2023.100508> (2023).

64. Gherraby, Y. et al. Application of aptenia cordifolia powder as a biosorbent for methylene blue retention from an aqueous medium: isotherm, kinetic, and thermodynamic investigations. *Desalin. Water Treat.* **318**, 100263. <https://doi.org/10.1016/j.dwt.2024.100263> (2024).
65. Iqajtaoune, A., Taibi, M., Saufi, H., Aouan, B. & Boudad, L. Enhanced removal of methylene blue and Procion deep red H-EXL dyes from aqueous environments by modified-bentonite: isotherm, kinetic, and thermodynamic. *Desalin. Water Treat.* **320**, 100607. <https://doi.org/10.1016/j.dwt.2024.100607> (2024).
66. Cheriaa, J., Khairredine, M., Rouabhia, M. & Bakhrrouf, A. Removal of triphenylmethane dyes by bacterial consortium. *Sci. World J.* **2012** 512454. <https://doi.org/10.1100/2012/512454> (2012).
67. Kazak, O., Eker, Y. R., Akin, I., Bingol, H. & Tor, A. A novel red mud@sucrose based carbon composite: preparation, characterization and its adsorption performance toward methylene blue in aqueous solution. *J. Environ. Chem. Eng.* **5**, 2639–2647. <https://doi.org/10.1016/j.jece.2017.05.018> (2017).
68. Aouan, B. et al. The Dye-Contaminated water treatment efficiency of two types of geopolymers: A comparative study of structural, microstructural and adsorption properties. *J. Inorg. Organomet. Polym.* **35**, 1819–1844. <https://doi.org/10.1007/s10904-024-03399-4> (2025).
69. Karuppaiyan, J., Mullaimalar, A. & Jeyalakshmi, R. Adsorption of dyestuff by nano copper oxide coated alkali metakaoline geopolymer in monolith and powder forms: kinetics, isotherms and microstructural analysis. *Environ. Res.* **218**, 115002. <https://doi.org/10.1016/j.envres.2022.115002> (2023).
70. Elshimy, A. S. et al. Utilization of alkali-activated dolomite waste toward the fabrication of an effective adsorbent: experimental study and statistical physics formalism for the removal of methylene blue and crystal Violet. *J. Phys. Chem. Solids.* **180**, 111442. <https://doi.org/10.1016/j.jpcs.2023.111442> (2023).
71. Siyal, A. A., Shamsuddin, M. R., Khahro, S. H., Low, A. & Ayoub, M. Optimization of synthesis of geopolymer adsorbent for the effective removal of anionic surfactant from aqueous solution. *J. Environ. Chem. Eng.* **9**, 104949. <https://doi.org/10.1016/j.jclepro.2022.131278> (2021).
72. Li, C. J., Zhang, Y. J., Chen, H., He, P. Y. & Meng, Q. Development of porous and reusable geopolymer adsorbents for dye wastewater treatment. *J. Clean. Prod.* **348**, 131278. <https://doi.org/10.1016/j.jece.2020.104949> (2022).
73. Jadhav, S. K. & Thorat, R. Adsorption isotherm study of crystal Violet dye onto Biochar prepared from agriculture waste. *Orient. J. Chem.* **38**, 475–481. <https://doi.org/10.13005/ojc/380234> (2022).
74. Tchakounte, A. et al. RSM-CCD design of volcanic Ash/ rice husk Ash based phosphate geopolymer for crystal Violet adsorption: kinetics and isotherms. *Sci. Rep.* **14**, 29422. <https://doi.org/10.1038/s41598-024-79017-7> (2024).
75. Barbosa, T. R., Foletto, E. L., Dotto, G. L. & Jahn, S. L. Preparation of mesoporous geopolymer using Metakaolin and rice husk Ash as synthesis precursors and its use as potential adsorbent to remove organic dye from aqueous solutions. *Ceram. Int.* **44**, 416–423. <https://doi.org/10.1016/j.ceramint.2017.09.193> (2018).
76. Sen, N. et al. Adsorption of crystal Violet dye from synthetic wastewater by ball-milled Royal palm leaf sheath. *Sci. Rep.* **14**, 5349. <https://doi.org/10.1038/s41598-024-52395-8> (2024).
77. Yilmazoglu, M., Kanmaz, N. & Demircivi, P. Constructing the synergistic effects of Chitosan and ionic liquid on SPEEK polymer for efficient adsorption of crystal Violet dye. *Int. J. Biol. Macromol.* **271**, 132638. <https://doi.org/10.1016/j.ijbiomac.2024.132638> (2024).

Acknowledgements

The authors express their gratitude to the Desert Research Center and the Central Labs of Ain Shams University in Cairo, Egypt, for their support in supplying the chemical analysis data for this study. The authors express their gratitude to Prof. Dr/ Eisa E. Heakl for his assistance in explaining some study results.

Author contributions

Essam A. Kishar: Conceptualization, Methodology, Supervision. Doaa A. Ahmed: Conceptualization, Methodology, Investigation, Software, Writing – Reviewing & Editing, Supervision. Aya Allah M. Ebrahim: Methodology, Investigation, Formal analysis, Writing – original draft, Supervision. Soher A. Hashish: Methodology, Investigation, Formal analysis, Writing – original draft Writing – Reviewing & Editing. Sheren M. Ragei Investigation, Formal analysis, Supervision. All authors read and approved the final manuscript.

Funding

Open access funding provided by The Science, Technology & Innovation Funding Authority (STDF) in cooperation with The Egyptian Knowledge Bank (EKB). Not applicable.

Declarations

Competing interests

The authors declare no competing interests.

Additional information

Correspondence and requests for materials should be addressed to S.A.H.

Reprints and permissions information is available at www.nature.com/reprints.

Publisher's note Springer Nature remains neutral with regard to jurisdictional claims in published maps and institutional affiliations.

Open Access This article is licensed under a Creative Commons Attribution 4.0 International License, which permits use, sharing, adaptation, distribution and reproduction in any medium or format, as long as you give appropriate credit to the original author(s) and the source, provide a link to the Creative Commons licence, and indicate if changes were made. The images or other third party material in this article are included in the article's Creative Commons licence, unless indicated otherwise in a credit line to the material. If material is not included in the article's Creative Commons licence and your intended use is not permitted by statutory regulation or exceeds the permitted use, you will need to obtain permission directly from the copyright holder. To view a copy of this licence, visit <http://creativecommons.org/licenses/by/4.0/>.

© The Author(s) 2025